

# Functional renormalization group for Luttinger liquids with impurities

S. Andergassen,<sup>1</sup> T. Enss,<sup>1</sup> V. Meden,<sup>2</sup> W. Metzner,<sup>1</sup>  
U. Schollwöck,<sup>3</sup> and K. Schönhammer<sup>2</sup>

<sup>1</sup>*Max-Planck-Institut für Festkörperforschung, D-70569 Stuttgart, Germany*

<sup>2</sup>*Institut für Theoretische Physik, Universität Göttingen, D-37077 Göttingen, Germany*

<sup>3</sup>*Institut für Theoretische Physik, Technische Hochschule Aachen, D-52056 Aachen, Germany*

(Dated: March 19, 2004)

We improve the recently developed functional renormalization group (fRG) for impurities and boundaries in Luttinger liquids by including renormalization of the two-particle interaction, in addition to renormalization of the impurity potential. Explicit flow equations are derived for spinless lattice fermions with nearest neighbor interaction at zero temperature, and a fast algorithm for solving these equations for very large systems is presented. We compute spectral properties of single-particle excitations, and the oscillations in the density profile induced by impurities or boundaries for chains with up to  $10^6$  lattice sites. The expected asymptotic power-laws at low energy or long distance are fully captured by the fRG. Results on the relevant energy scales and crossover phenomena at intermediate scales are also obtained. A comparison with numerical density matrix renormalization results for systems with up to 1000 sites shows that the fRG with the inclusion of vertex renormalization is remarkably accurate even for intermediate interaction strengths.

PACS: 71.10.Pm, 72.10.-d, 73.21.Hb

## I. INTRODUCTION

Low dimensional electron systems exhibit a rich variety of surprising effects which are due to the cooperative interplay of impurities and interactions. In one dimension even clean metallic systems are always strongly affected by interactions: at low energy scales physical properties obey anomalous power-laws, known as Luttinger liquid behavior, which is very different from the conventional Fermi liquid behavior describing most higher dimensional metals.<sup>1,2</sup> In Luttinger liquids with repulsive interactions already a single static impurity is known to affect the low-energy properties drastically.<sup>3,4,5,6,7,8,9</sup> The impurity potential in a repulsive Luttinger liquid becomes dressed by long-range oscillations which suppress the spectral weight for single-particle excitations near the impurity and also the conductance through the impurity down to zero in the low-energy limit.

The *asymptotic* low-energy properties of Luttinger liquids with a single impurity are rather well understood. Universal power-laws and scaling functions have been obtained by

bosonization, conformal field theory, and exact solutions for the low-energy asymptotics in special integrable cases.<sup>10</sup> What remains to be developed, however, is a many-body method for *microscopic* models of interacting fermions with impurities, which does not only capture correctly the universal low-energy asymptotics, but allows one to compute observables on all energy scales, providing thus also *non-universal* properties, and in particular an answer to the important question at what *scale* the ultimate asymptotics sets in. That scale can indeed be surprisingly low, and the properties above it very different from the asymptotic behavior. Some of the non-universal properties can be computed numerically by the density matrix renormalization group (DMRG),<sup>11</sup> but this method is limited to lattice systems with about 1000 sites, and only a restricted set of observables can be evaluated with affordable computational effort.

In the last few years it has been realized that the functional renormalization group (fRG) is a source of powerful new computation tools for interacting Fermi systems, especially for low-dimensional systems with competing instabilities and entangled infrared singularities. The starting point of this approach is an exact hierarchy of differential flow equations for the Green or vertex functions of the system, which is obtained by taking derivatives with respect to an infrared cutoff  $\Lambda$ .<sup>12</sup> Approximations are then constructed by truncating the hierarchy and parametrizing the vertex functions with a manageable set of variables or functions.<sup>13</sup>

A relatively simple fRG approximation for impurities in spinless Luttinger liquids has been developed recently by some of us.<sup>14</sup> The scheme starts from an fRG hierarchy for one-particle irreducible vertex functions, as first derived in a field theoretical context by Wetterich<sup>15</sup> and Morris,<sup>16</sup> and for interacting Fermi systems by Salmhofer and Honerkamp.<sup>17</sup> A Matsubara frequency cutoff is used as the flow parameter. The hierarchy is then truncated already at first order, such that the 2-particle vertex remains unrenormalized, and the flow of the self-energy, which describes the renormalized impurity potential, is determined by the bare 2-particle interaction. No simplified parametrization of the self-energy is necessary such that the full spatial dependence of the renormalized impurity potential can be obtained for very large lattice systems. In spite of the striking simplicity of this scheme it was shown that the effects of a single static impurity in a spinless Luttinger liquid are fully captured qualitatively, and in the weak coupling limit also quantitatively.<sup>14</sup> In particular, one obtains that impurity potentials in repulsive Luttinger liquids become effectively stronger at lower energy scales, and act ultimately as a weak link between two otherwise separate wires, as predicted by Kane and Fisher.<sup>7</sup> The fRG also correctly yields the universal low energy power-laws with exponents that do not depend on the bare impurity strength. In addition, it was shown that the asymptotic behavior holds typically only at very low energy scales and for very large systems, except for very strong bare impurities.<sup>14</sup> The fRG approach to impurities in Luttinger liquids was originally developed and tested for spectral densities of single-particle excitations, but has been applied very recently also to transport problems, such as persistent

currents in mesoscopic rings<sup>18,19</sup> and the conductance of interacting wires connected to non-interacting leads.<sup>19,20</sup> The full power of the fRG with its ability to deal naturally also with complex crossover phenomena emerges most convincingly in the multi-scale problem posed by the transport through a resonant double barrier.<sup>21</sup>

In the present work we further develop the fRG approach for impurities in Luttinger liquids by including 2-particle vertex renormalization, that is we go one step further in the hierarchy of flow equations than previously.<sup>22</sup> For spinless fermions this extension does not matter qualitatively, as the lowest order is already qualitatively correct, but the quantitative accuracy of the results improves considerably in particular at intermediate interaction strengths. For spin- $\frac{1}{2}$  systems, which we will treat in a subsequent work,<sup>23</sup> vertex renormalization is necessary to take into account that backscattering of particles with opposite spins at opposite Fermi points scales to zero in the low energy limit. A crucial point is to devise an efficient parametrization of the vertex by a manageable number of variables. Here we focus on spinless lattice fermions with nearest neighbor interaction as a prototype model. The bulk model is supplemented by site or hopping impurities. We also analyze the influence of boundaries, which can be viewed as infinite barriers or infinitesimal weak links. We choose to parametrize the vertex by a renormalized nearest neighbor interaction, which allows us to capture various advantageous features: the low energy flow of the vertex at  $k_F$  in the pure system is obtained correctly to second order in the renormalized couplings; the non-universal contributions at finite energy scales are correct to second order in the bare interaction; the algorithm for the flow of the self-energy remains as fast as in the absence of vertex renormalization, such that one can easily deal with up to  $10^6$  lattice sites. We compute spectral properties of single-particle excitations near an impurity and the oscillations in the density profile induced by an impurity, or by a boundary. The accuracy of the calculation is checked by comparing with DMRG results for systems with up to 1000 lattice sites and with exact results for the asymptotic behavior, which can be obtained from the Bethe ansatz and bosonization.

The article is structured as follows. In Sec. II we introduce the microscopic model and various types of impurities. The fRG formalism is developed in Sec. III, and worked out explicitly for the spinless fermion model with nearest neighbor interaction. Sec. IV is dedicated to results for the renormalized impurity potential, spectral properties, and the density profile. We finally conclude in Sec. V with an outline of promising extensions of the present work.

## II. MICROSCOPIC MODEL

We consider the spinless fermion lattice model with nearest neighbor interaction and various types of impurity potentials. The Hamiltonian has the form

$$H = H_0 + H_I + H_{\text{imp}} \quad (1)$$

where the kinetic energy

$$H_0 = -t \sum_j (c_{j+1}^\dagger c_j + c_j^\dagger c_{j+1}) \quad (2)$$

is given by nearest neighbor hopping with an amplitude  $t$ , and

$$H_I = U \sum_j n_j n_{j+1} \quad (3)$$

is a nearest neighbor interaction of strength  $U$ . We use standard second quantization notation, where  $c_j^\dagger$  and  $c_j$  are creation and annihilation operators on site  $j$ , respectively, and  $n_j = c_j^\dagger c_j$  is the local density operator. The impurity is represented by

$$H_{\text{imp}} = \sum_{j,j'} V_{j'j} c_{j'}^\dagger c_j \quad (4)$$

where  $V_{j'j}$  is a static potential. For "site impurities"

$$V_{j'j} = V_j \delta_{jj'} \quad (5)$$

this potential is local. For the important special case of a single site impurity

$$V_j = V \delta_{jj_0} \quad (6)$$

the potential acts only on one site  $j_0$ . We also consider "hopping impurities" described by the non-local potential

$$V_{j'j} = V_{jj'} = -t_{j,j+1} \delta_{j',j+1} . \quad (7)$$

For the special case of a single hopping impurity,

$$t_{j,j+1} = (t' - t) \delta_{jj_0} , \quad (8)$$

the hopping amplitude  $t$  is replaced by  $t'$  on the bond linking the sites  $j_0$  and  $j_0 + 1$ . In the following we will set the bulk hopping amplitude  $t$  equal to one, that is all energies are given in units of  $t$ .

The clean spinless fermion model  $H_0 + H_I$  is exactly solvable via the Bethe ansatz.<sup>24</sup> The system is a Luttinger liquid for all particle densities  $n$  and any interaction strength except at half-filling for  $|U| > 2$ . For  $U > 2$  a charge density wave with wave vector  $\pi$  forms, for  $U < -2$  the system undergoes phase separation. The Luttinger liquid parameter  $K_\rho$ , which determines all the critical exponents of the liquid, can be computed exactly from the Bethe ansatz solution.<sup>25</sup> At half-filling  $K_\rho$  is related to  $U$  by the simple explicit formula

$$K_\rho^{-1} = \frac{2}{\pi} \arccos \left( -\frac{U}{2} \right) \quad (9)$$

for  $|U| \leq 2$ .

We will compute physical properties for the above models on finite chains with open boundary conditions. The fRG equations can be solved easily for chains with up to  $10^6$  sites, the DMRG can be applied for up to  $10^3$  sites. To avoid oscillations emerging from the ends of the chain we will sometimes attach non-interacting semi-infinite leads to the finite interacting chain, with a smoothly decaying interaction at the contact.

### III. FUNCTIONAL RENORMALIZATION GROUP

This section is dedicated to a detailed presentation of the fRG equations for one-dimensional Fermi systems with impurities, including vertex renormalization, at zero temperature. We use the one-particle irreducible version of the functional RG.<sup>15,16</sup> The starting point is an exact hierarchy of flow equations for the irreducible vertex functions, which is obtained by cutting off the infrared part of the free propagator on a scale  $\Lambda$ , and differentiating the generating functional for the vertex functions with respect to this scale.<sup>17</sup>

#### A. Cutoff and flow equations

The cutoff can be imposed in many different ways. The only requirement is that the infrared singularities must be regularized such that the flow equations allow for a regular perturbation expansion in powers of the renormalized two-particle vertex. For our purposes a sharp Matsubara frequency cutoff is the most efficient choice. A momentum cutoff is less suitable here since the impurity spoils momentum conservation. The cutoff is imposed by excluding modes with frequencies below scale  $\Lambda$  from the functional integral representation of the system, or equivalently, by introducing a regularized bare propagator

$$G_0^\Lambda(i\omega) = \Theta(|\omega| - \Lambda) G_0(i\omega) . \quad (10)$$

Here  $G_0$  is the bare propagator of the pure system, involving neither interactions nor impurities. Instead of the sharp cutoff imposed by the step function  $\Theta$  one may also choose a smooth cutoff function, but the sharp cutoff has the advantage that it reduces the number of integration variables on the right hand side of the flow equations. Note that we will frequently write expressions which are well defined only if the sharp cutoff is viewed as a limit of increasingly sharp smooth cutoff functions. The suppression of frequencies below scale  $\Lambda$  affects all Green and vertex functions of the interacting system, which become thus functions of  $\Lambda$ . The original system is recovered in the limit  $\Lambda \rightarrow 0$ .

The first two equations in the exact hierarchy of flow equations for the one-particle irreducible  $m$ -particle vertex functions are depicted graphically in Figs. 1 and 2. The first equation yields the flow of the self-energy, which is related to the interacting propagator

by the usual Dyson equation

$$G^\Lambda = [(G_0^\Lambda)^{-1} - \Sigma^\Lambda]^{-1} . \quad (11)$$

Here and below  $G^\Lambda$ ,  $\Sigma^\Lambda$  etc. are operators, which do not refer to any particular single-particle basis, unless we write matrix indices explicitly. The right hand side of the flow equation involves the 2-particle vertex  $\Gamma^\Lambda$ , and the so-called single scale propagator  $S^\Lambda$  defined as

$$S^\Lambda = G^\Lambda [\partial_\Lambda (G_0^\Lambda)^{-1}] G^\Lambda = - \frac{1}{1 - G_0^\Lambda \Sigma^\Lambda} \frac{\partial G_0^\Lambda}{\partial \Lambda} \frac{1}{1 - \Sigma^\Lambda G_0^\Lambda} . \quad (12)$$

Note that  $S^\Lambda$  has support only on a single frequency scale:  $|\omega| = \Lambda$ . The precise flow equation for the self-energy (sketched graphically in Fig. 1) reads

$$\frac{\partial}{\partial \Lambda} \Sigma^\Lambda(1', 1) = - \frac{1}{\beta} \sum_{2, 2'} e^{i\omega_2 0^+} S^\Lambda(2, 2') \Gamma^\Lambda(1', 2'; 1, 2) , \quad (13)$$

where  $\beta$  is the inverse temperature. The numbers 1, 2, etc. are a shorthand for Matsubara frequencies and labels for single-particle states such as site and spin indices. Note that  $\omega_1 = \omega'_1$  and  $\omega_2 = \omega'_2$  due to Matsubara frequency conservation. The exponential factor in the above equation is irrelevant at any finite  $\Lambda$ , but is necessary to define the initial conditions of the flow at  $\Lambda = \Lambda_0 \rightarrow \infty$  (see below).

The right hand side of the flow equation for the 2-particle vertex  $\Gamma^\Lambda$ , shown in Fig. 2, involves  $\Gamma^\Lambda$  itself, but also the 3-particle vertex  $\Gamma_3^\Lambda$ . The latter could be computed from a flow equation involving the 4-particle vertex  $\Gamma_4^\Lambda$ , and so on. To avoid this unmanageable proliferation of vertex functions we make our first approximation: we neglect the contribution of the 3-particle vertex to the flow of  $\Gamma^\Lambda$ . The coupled system of flow equations for  $\Gamma^\Lambda$  and  $\Sigma^\Lambda$  is then closed. The contribution of  $\Gamma_3^\Lambda$  to  $\Gamma^\Lambda$  is small as long as  $\Gamma^\Lambda$  is sufficiently small, because  $\Gamma_3^\Lambda$  is initially (at  $\Lambda_0$ ) zero and is generated only from terms of third order in  $\Gamma^\Lambda$ .<sup>17</sup> A comparison of the RG results to exact DMRG results and exact scaling properties shows that the truncation error is often surprisingly small even for rather large interactions.<sup>14</sup> The explicit form of the truncated flow equation for the 2-particle vertex reads

$$\begin{aligned} \frac{\partial}{\partial \Lambda} \Gamma^\Lambda(1', 2'; 1, 2) = & \frac{1}{\beta} \sum_{3, 3'} \sum_{4, 4'} G^\Lambda(3, 3') S^\Lambda(4, 4') \\ & \times \left[ \Gamma^\Lambda(1', 2'; 3, 4) \Gamma^\Lambda(3', 4'; 1, 2) \right. \\ & - \Gamma^\Lambda(1', 4'; 1, 3) \Gamma^\Lambda(3', 2'; 4, 2) - (3 \leftrightarrow 4, 3' \leftrightarrow 4') \\ & \left. + \Gamma^\Lambda(2', 4'; 1, 3) \Gamma^\Lambda(3', 1'; 4, 2) + (3 \leftrightarrow 4, 3' \leftrightarrow 4') \right] \quad (14) \end{aligned}$$

The various contributions are shown diagrammatically in Fig. 3.

For a sharp frequency cutoff the frequency sums on the right hand side of the flow equations can be carried out analytically in the zero temperature limit, where the Matsubara sums become integrals. At this point one has to deal with products of delta functions  $\delta(|\omega| - \Lambda)$  and expressions involving step functions  $\Theta(|\omega| - \Lambda)$ . These at first sight ambiguous expressions are well defined and unique if the sharp cutoff is implemented as a limit of increasingly sharp broadened cutoff functions  $\Theta_\epsilon$ , with the broadening parameter  $\epsilon$  tending to zero. The expressions can then be conveniently evaluated by using the following relation,<sup>16</sup> valid for arbitrary continuous functions  $f$ :

$$\delta_\epsilon(x - \Lambda) f[\Theta_\epsilon(x - \Lambda)] \rightarrow \delta(x - \Lambda) \int_0^1 f(t) dt, \quad (15)$$

where  $\delta_\epsilon = \Theta'_\epsilon$ . Note that the functional form of  $\Theta_\epsilon$  for finite  $\epsilon$  does not affect the result in the limit  $\epsilon \rightarrow 0$ .

Instead of writing down the frequency-integrated flow equations in full generality, we first implement our second approximation: the frequency dependent flow of the renormalized 2-particle vertex  $\Gamma^\Lambda$  is replaced by its value at vanishing (external) frequencies, such that  $\Gamma^\Lambda$  remains frequency independent. As a consequence, also the self-energy becomes frequency independent. Since the bare interaction is frequency independent, neglecting the frequency dependence leads to errors only at second order (in the interaction strength) for the self-energy, and at third order for the vertex function at zero frequency. Besides the quantitative errors we miss qualitative properties related to the frequency dependence of the self-energy, such as the suppression of the one-particle spectral weight in the bulk of a pure Luttinger liquid. On the other hand, a comparison with exact numerical results and asymptotic analytical results shows that the impurity effects are not qualitatively affected by the frequency dependence of  $\Sigma$ , at least for weak interactions.

Carrying out the frequency integration in the flow equation for the self-energy, and inserting a frequency independent 2-particle vertex, one obtains

$$\frac{\partial}{\partial \Lambda} \Sigma_{1',1}^\Lambda = -\frac{1}{2\pi} \sum_{\omega=\pm\Lambda} \sum_{2,2'} e^{i\omega 0^+} \tilde{G}_{2,2'}^\Lambda(i\omega) \Gamma_{1',2';1,2}^\Lambda, \quad (16)$$

where the lower indices 1, 2, etc. label single-particle states (not frequencies) and

$$\tilde{G}^\Lambda(i\omega) = [G_0^{-1}(i\omega) - \Sigma^\Lambda]^{-1}. \quad (17)$$

Note that  $\tilde{G}^\Lambda$  has no jump at  $|\omega| = \Lambda$ , in contrast to  $G^\Lambda$ . The frequency integrated flow equation for the 2-particle vertex, evaluated at vanishing external frequencies, has the form

$$\begin{aligned} \frac{\partial}{\partial \Lambda} \Gamma_{1',2';1,2}^\Lambda = & \frac{1}{2\pi} \sum_{\omega=\pm\Lambda} \sum_{3,3'} \sum_{4,4'} \left[ \frac{1}{2} \tilde{G}_{3,3'}^\Lambda(i\omega) \tilde{G}_{4,4'}^\Lambda(-i\omega) \Gamma_{1',2';3,4}^\Lambda \Gamma_{3',4';1,2}^\Lambda \right. \\ & \left. + \tilde{G}_{3,3'}^\Lambda(i\omega) \tilde{G}_{4,4'}^\Lambda(i\omega) (-\Gamma_{1',4';1,3}^\Lambda \Gamma_{3',2';4,2}^\Lambda + \Gamma_{2',4';1,3}^\Lambda \Gamma_{3',1';4,2}^\Lambda) \right] \quad (18) \end{aligned}$$

The flow is determined uniquely by the differential flow equations and the initial conditions at  $\Lambda = \infty$ . For  $\Lambda = \infty$  the vertex functions are given by the bare interactions of the system. In particular, the flow of the 2-particle vertex starts from the antisymmetrized bare 2-particle interaction while  $m$ -particle vertices of higher order vanish at  $\Lambda = \infty$ , in the absence of  $m$ -body interactions with  $m > 2$ . The self-energy at  $\Lambda = \infty$  is given by the bare one-particle potential, that is by those one-particle terms which are not included already in  $G_0$ . We choose to include the translationally invariant bulk kinetic energy and the chemical potential in  $G_0$ , while the impurity (site or hopping) potential  $V$  is assigned to the initial condition of the self-energy. In a numerical solution the flow starts at some large finite initial cutoff  $\Lambda_0$ . Here one has to take into account that, due to the slow decay of the right hand side of the flow equation for  $\Sigma^\Lambda$  at large  $\Lambda$ , the integration of the flow from  $\Lambda = \infty$  to  $\Lambda = \Lambda_0$  yields a contribution which does not vanish in the limit  $\Lambda_0 \rightarrow \infty$ , but rather tends to a finite constant. Since  $\tilde{G}_{2,2'}^\Lambda(i\omega) \rightarrow \delta_{2,2'}/(i\omega)$  for  $|\omega| = \Lambda \rightarrow \infty$ , this constant is easily determined as

$$-\frac{1}{2\pi} \lim_{\Lambda_0 \rightarrow \infty} \int_{\infty}^{\Lambda_0} d\Lambda \sum_{\omega=\pm\Lambda} \sum_{2,2'} e^{i\omega 0^+} \frac{\delta_{2,2'}}{i\omega} I_{1',2';1,2} = \frac{1}{2} \sum_2 I_{1',2;1,2}, \quad (19)$$

where  $I_{1',2';1,2}$  is the bare antisymmetrized interaction. In summary, the initial conditions for the self-energy and the 2-particle vertex at  $\Lambda = \Lambda_0 \rightarrow \infty$  are

$$\Sigma_{1,1'}^{\Lambda_0} = V_{1,1'} + \frac{1}{2} \sum_2 I_{1',2;1,2} \quad (20)$$

$$\Gamma_{1',2';1,2}^{\Lambda_0} = I_{1',2';1,2}, \quad (21)$$

where  $V_{1,1'}$  is the bare impurity potential. For the flow at  $\Lambda < \Lambda_0$  the factor  $e^{i\omega 0^+}$  in Eq. (16) can be discarded.

## B. Parametrization of 2-particle vertex

For a finite lattice system with  $L$  sites the flow of the 2-particle vertex  $\Gamma_{1',2';1,2}^\Lambda$  involves  $\mathcal{O}(L^3)$  independent flowing variables, if translation invariance is assumed, and  $\mathcal{O}(L^4)$  variables, if the influence of the impurity on the flow of the 2-particle vertex is taken into account. For a treatment of large systems it is therefore necessary to reduce the number of variables by a suitable approximate parametrization of the vertex. In the low energy limit (small  $\Lambda$ ) the flow is dominated by a very small number of variables anyway, the others being irrelevant according to standard RG arguments.<sup>2</sup> In particular, the frequency dependence of the vertex, discarded already above, is irrelevant for the flow of  $\Gamma^\Lambda$  at small  $\Lambda$ . For larger  $\Lambda$  one can use perturbation theory as a guide for a simple but efficient parametrization of  $\Gamma^\Lambda$ .

We neglect the feedback of the self-energy into the flow of  $\Gamma^\Lambda$  and replace  $\tilde{G}^\Lambda$  by  $G_0$  in Eq. (18). The renormalization of  $\Gamma^\Lambda$  includes thus only bulk, not impurity, contributions,



such that  $\Gamma^\Lambda$  remains translation invariant. While this turns out to be sufficient for capturing the effects of isolated impurities in otherwise pure systems, it is known that impurity contributions to vertex renormalization become important in macroscopically disordered systems.<sup>26</sup> For a more concrete treatment of the vertex renormalization, we have to focus on a specific model. In this article we restrict ourselves to the spinless fermion model with nearest neighbor interaction, leaving an extension to spin- $\frac{1}{2}$  systems with more general interactions for subsequent work.<sup>23</sup>

For spinless fermions the 2-particle vertex and the self-energy are fully characterized by either site or momentum variables. In the low energy limit, the flow of the vertex is dominated by contributions with momenta close to the Fermi points, such that the right hand side of the flow equation is determined by momentum components of the vertex  $\Gamma_{k'_1, k'_2; k_1, k_2}^\Lambda$  with  $k_1, k_2, k'_1, k'_2 = \pm k_F$ . Due to the antisymmetry of the vertex, there is only one such component which is non-zero:

$$g^\Lambda = \Gamma_{k_F, -k_F; k_F, -k_F}^\Lambda. \quad (22)$$

In the low energy limit the momentum dependence of the vertex away from  $\pm k_F$  is irrelevant. There are therefore many possible choices for the functional form of  $\Gamma_{k'_1, k'_2; k_1, k_2}^\Lambda$ , which all lead to the correct low energy asymptotics. For a model with a bare nearest neighbor interaction  $U$ , a natural and efficient choice is to parametrize the flowing vertex simply by a renormalized nearest neighbor interaction  $U^\Lambda$ , which leads to a real space vertex of the form

$$\Gamma_{j'_1, j'_2; j_1, j_2}^\Lambda = U_{j_1, j_2}^\Lambda (\delta_{j_1, j'_1} \delta_{j_2, j'_2} - \delta_{j_1, j'_2} \delta_{j_2, j'_1}) \quad (23)$$

with  $U_{j_1, j_2}^\Lambda = U^\Lambda (\delta_{j_1, j_2-1} + \delta_{j_1, j_2+1})$ . This yields the following structure in momentum space:

$$\Gamma_{k'_1, k'_2; k_1, k_2}^\Lambda = 2U^\Lambda [\cos(k'_1 - k_1) - \cos(k'_2 - k_1)] \delta_{k_1+k_2, k'_1+k'_2}^{(2\pi)}, \quad (24)$$

where the Kronecker delta implements momentum conservation (modulo  $2\pi$ ). The flowing coupling constant  $U^\Lambda$  is linked to the value of the vertex at the Fermi points by the relation

$$g^\Lambda = 2U^\Lambda [1 - \cos(2k_F)]. \quad (25)$$

The flow equation for  $g^\Lambda$  becomes

$$\frac{\partial g^\Lambda}{\partial \Lambda} = \frac{1}{2\pi} \sum_{\omega=\pm\Lambda} \int \frac{dp}{2\pi} (\text{PP} + \text{PH} + \text{PH}') \quad (26)$$

with the particle-particle and particle-hole contributions

$$\begin{aligned} \text{PP} &= \frac{1}{2} G_p^0(i\omega) G_{-p}^0(-i\omega) \Gamma_{k_F, -k_F; p, -p}^\Lambda \Gamma_{p, -p; k_F, -k_F}^\Lambda \\ \text{PH} &= -[G_p^0(i\omega)]^2 \Gamma_{k_F, p; k_F, p}^\Lambda \Gamma_{p, -k_F; p, -k_F}^\Lambda \\ \text{PH}' &= G_{p-k_F}^0(i\omega) G_{p+k_F}^0(i\omega) \Gamma_{-k_F, p+k_F; k_F, p-k_F}^\Lambda \Gamma_{p-k_F, k_F; p+k_F, -k_F}^\Lambda, \end{aligned} \quad (27)$$

where  $\Gamma^\Lambda$  on the right hand side of the flow equation is given by Eq. (24). Using Eq. (25) to replace  $\partial_\Lambda g^\Lambda$  by  $\partial_\Lambda U^\Lambda$  on the left hand side of Eq. (26), one obtains a flow equation for  $U^\Lambda$  of the simple form

$$\partial_\Lambda U^\Lambda = h(\Lambda) (U^\Lambda)^2. \quad (28)$$

The function  $h(\Lambda)$  depends only on the cutoff  $\Lambda$  and the Fermi momentum  $k_F$ . An explicit formula for  $h(\Lambda)$  can be obtained by carrying out the momentum integral in Eq. (26) using the residue theorem, as sketched in Appendix A. For finite systems the momentum integral should be replaced by a discrete momentum sum; however, this leads to sizable corrections only for very small systems. The flow equation (28) can be integrated to

$$U^\Lambda = \frac{U}{1 - U H(\Lambda)}, \quad (29)$$

where  $H(\Lambda)$  is the primitive function of  $h(\Lambda)$  with  $H(\Lambda) \rightarrow 0$  for  $\Lambda \rightarrow \infty$ . Integrating  $h(\Lambda)$  one obtains

$$\begin{aligned} H(\Lambda) = & -\frac{\Lambda}{2\pi} + \frac{1}{\pi} \operatorname{Re} \left[ \frac{(4 - \mu_0^2)\Lambda^2 - 2i\mu_0(2 - \mu_0^2)\Lambda + \mu_0^4 - 6\mu_0^2 + 8}{2(4 - \mu_0^2)\sqrt{\Lambda^2 - 2i\mu_0\Lambda + 4 - \mu_0^2}} - \frac{i\mu_0}{2} \sinh^{-1} \frac{\Lambda - i\mu_0}{2} \right. \\ & \left. + \frac{\mu_0^4}{2(4 - \mu_0^2)^{3/2}} \tanh^{-1} \frac{4 + \mu_0^2 + i\mu_0\Lambda}{\sqrt{(4 + \mu_0^2 + i\mu_0\Lambda)^2 + 4(\Lambda - 2i\mu_0)^2}} \right], \end{aligned} \quad (30)$$

where  $\mu_0 = -2 \cos k_F$ , while  $\sinh^{-1}$  and  $\tanh^{-1}$  denote the main branch of the inverse of the complex functions  $\sinh$  and  $\tanh$ , respectively. At half-filling, corresponding to  $k_F = \pi/2$ , the function  $h(\Lambda)$  is particularly simple (see Appendix A), such that also  $U^\Lambda$  has a relatively simple form:

$$U^\Lambda = \frac{U}{1 + \left( \Lambda - \frac{2+\Lambda^2}{\sqrt{4+\Lambda^2}} \right) U/(2\pi)}. \quad (31)$$

In Fig. 4 we show results for the renormalized nearest neighbor interaction  $U^\Lambda$  as obtained from the flow equation at various densities  $n$ , for a bare interaction  $U = 1$ . While the renormalization does not follow any simple rule at intermediate scales  $\Lambda$ , all curves saturate at a finite value  $U^*$  in the limit  $\Lambda \rightarrow 0$ , corresponding to a finite  $g^*$ , as expected for a Luttinger liquid fixed point.<sup>2</sup>

The above simplified flow equation yields not only the correct low energy asymptotics to second order in the renormalized vertex, but contains also all *non-universal* second order corrections to the vertex at  $\pm k_F$  at higher energy scales. Hence the resulting fixed point coupling  $g^*$ , from which the Luttinger liquid parameter  $K_\rho$  can be computed, is obtained correctly to second order in  $U$ . The calculation of  $K_\rho$ , presented in Appendix B, illustrates how Luttinger liquid parameters can be related to the fixed point couplings obtained from the fRG. A comparison of the RG result for  $K_\rho$  with exact results from the Bethe ansatz solution of the spinless fermion model shows that the vertex renormalization scheme described above is not only very simple, but also surprisingly accurate.

Parametrizing  $\Gamma^\Lambda$  by a renormalized nearest neighbor interaction has the enormous advantage that the self-energy, as determined by the flow equation (16), is a tridiagonal matrix in real space, that is only the matrix elements  $\Sigma_{j,j}^\Lambda$  and  $\Sigma_{j,j\pm 1}^\Lambda$  are non-zero. Inserting  $\Gamma^\Lambda$  from Eq. (23) into (16), one obtains the following simple coupled flow equations for the diagonal and off-diagonal matrix elements:

$$\begin{aligned}\frac{\partial}{\partial\Lambda}\Sigma_{j,j}^\Lambda &= -\frac{U^\Lambda}{2\pi}\sum_{\omega=\pm\Lambda}\sum_{r=\pm 1}\tilde{G}_{j+r,j+r}^\Lambda(i\omega) \\ \frac{\partial}{\partial\Lambda}\Sigma_{j,j\pm 1}^\Lambda &= \frac{U^\Lambda}{2\pi}\sum_{\omega=\pm\Lambda}\tilde{G}_{j,j\pm 1}^\Lambda(i\omega).\end{aligned}\tag{32}$$

Note that the self-energy enters also the right hand side of these equations, via  $\tilde{G}^\Lambda = (G_0^{-1} - \Sigma^\Lambda)^{-1}$ . Since  $\Sigma^\Lambda$  and  $G_0^{-1}$  are both tridiagonal in real space, the matrix inversion required to compute the diagonal and first off-diagonal elements of  $\tilde{G}^\Lambda$  from  $\Sigma^\Lambda$  can be carried out very efficiently, and thus for very large systems. In Appendix C we describe an algorithm for the numerical solution of the flow equation for  $\Sigma$  which scales only linearly with the size of the system.

### C. Observables

In the next section we will present results for spectral properties of single-particle excitations near an impurity or boundary, and for the density profile. Here we describe how the relevant observables are computed from the solution of the flow equations.

#### 1. Single-particle excitations

Integrating the flow equation for the self-energy  $\Sigma^\Lambda$  down to  $\Lambda = 0$  yields the physical (cutoff-free) self-energy  $\Sigma$ , and the single-particle propagator  $G = (G_0^{-1} - \Sigma)^{-1}$ . From the latter spectral properties of single-particle excitations can be extracted. We focus on local spectral properties, which are described by the *local spectral function*

$$\rho_j(\omega) = -\frac{1}{\pi}\text{Im} G_{jj}(\omega + i0^+),\tag{33}$$

where  $G_{jj}(\omega + i0^+)$  is the local propagator, analytically continued to the real frequency axis from above.

In our approximation the self-energy is frequency-independent and can therefore be viewed as an effective single-particle potential. The propagator  $G$  is thus the Green function of an effective single-particle Hamiltonian. In real space representation this Hamiltonian is given by the tridiagonal matrix  $h_{\text{eff}} = h_0 + \Sigma$ , where the matrix elements of  $h_0$  are the hopping amplitudes in  $H_0$ , Eq. (2). For a lattice with  $L$  sites this matrix has  $L$

(including possible multiplicities) eigenvalues  $\epsilon_\lambda$  and an orthonormal set of corresponding eigenvectors  $\psi_\lambda$ . For the spectral function  $\rho_j(\omega)$  one thus obtains a sum of  $\delta$ -functions

$$\rho_j(\omega) = \sum_{\lambda} w_{\lambda j} \delta(\omega - \xi_\lambda) , \quad (34)$$

where  $\xi_\lambda = \epsilon_\lambda - \mu$ , and the *spectral weight*  $w_{\lambda j}$  is the squared modulus of the amplitude of  $\psi_\lambda$  on site  $j$ . For large  $L$  the level spacing between neighboring eigenvalues is usually of order  $L^{-1}$ , except for one or a few levels outside the band edges which correspond to bound states.

Due to even-odd effects etc. the spectral weight  $w_{\lambda j}$  generally varies quickly from one eigenvalue to the next one. A smooth function of  $\omega$  which suppresses these usually irrelevant finite-size details can be obtained by averaging over neighboring eigenvalues. In addition it is useful to divide by the level spacing between eigenvalues to obtain the conventional local *density of states*, which we denote by  $D_j(\omega)$ .

## 2. Density profile

Boundaries or impurities induce a density profile with long-range Friedel oscillations, which are expected to decay with a power-law at long distances.<sup>28</sup> The expectation value of the local density  $n_j$  could be computed from the local one-particle propagator  $G_{jj}$ , if  $G$  was known exactly. However, the approximate flow equations for  $\Sigma$  can be expected to describe the asymptotic behavior of  $G$  correctly only at long distances between creation and annihilation operator in time and/or space, while in the local density operator time and space variables coincide. In the standard RG terminology  $n_j$  is a *composite* operator, which has to be renormalized separately.<sup>29</sup>

To derive a flow equation for  $n_j$ , we follow the usual procedure for the renormalization of correlation functions involving composite operators: we add a term  $\phi_j n_j$  with a small field  $\phi_j$  to the Hamiltonian, and take derivatives with respect to  $\phi_j$  in the flow equations. The local density is given by

$$n_j = \left. \frac{\partial \Omega(\phi_j)}{\partial \phi_j} \right|_{\phi_j=0} , \quad (35)$$

where  $\Omega(\phi_j)$  is the grand canonical potential of the system in the presence of the field  $\phi_j$ . Note that we use the same symbol  $n_j$  for the density operator and its expectation value. In the presence of a cutoff  $\Lambda$  the grand canonical potential obeys the exact flow-equation

$$\frac{\partial}{\partial \Lambda} \Omega^\Lambda = \frac{1}{\beta} \sum_{\omega} \text{tr} \left\{ e^{i\omega 0^+} [\partial_\Lambda G_0^\Lambda(i\omega)^{-1}] [G^\Lambda(i\omega) - G_0^\Lambda(i\omega)] \right\} \quad (36)$$

in a short-hand matrix notation. This flow-equation follows from the functional flow equation for the generating functional for vertex functions<sup>17</sup> and the relation between the grand canonical potential and the zero-particle vertex. At zero temperature the

Matsubara frequency sum becomes an integral which, for the sharp frequency cutoff (10), can be carried out analytically. This yields

$$\frac{\partial}{\partial \Lambda} \Omega^\Lambda = \frac{1}{2\pi} \sum_{\omega=\pm\Lambda} \text{tr} \left\{ e^{i\omega 0^+} \log[1 - G_0(i\omega) \Sigma^\Lambda(i\omega)] \right\} . \quad (37)$$

We attribute  $\phi_j$  to the "interaction" part of the Hamiltonian, not to  $H_0$ , such that  $G_0$  remains independent of  $\phi_j$ . The self-energy is modified via the additional local and frequency-independent contribution  $\phi_j \delta_{jj'}$  to its initial value  $\Sigma_{jj'}^{\Lambda_0}$  at scale  $\Lambda_0$ .

The density profile can be obtained from the above equations and the flow equation for  $\Sigma^\Lambda$  by computing the shift of  $\Omega$  generated by a small finite perturbation  $\phi_j$ , that is by numerical differentiation. Alternatively one may carry out the  $\phi_j$ -derivative analytically in the flow equations, which yields a flow equation for the density in terms of the density response vertex. Taking the  $\phi_j$  derivative in (37) yields

$$\frac{\partial}{\partial \Lambda} n_j^\Lambda = -\frac{1}{2\pi} \sum_{\omega=\pm\Lambda} \text{tr} \left[ e^{i\omega 0^+} \tilde{G}^\Lambda(i\omega) R_j^\Lambda(i\omega) \right] \quad (38)$$

with the density response vertex

$$R_j^\Lambda(i\omega) = \left. \frac{\partial \Sigma^\Lambda(i\omega)}{\partial \phi_j} \right|_{\phi_j=0} , \quad (39)$$

where the propagator  $\tilde{G}^\Lambda$  is computed as previously, that is in the absence of  $\phi_j$ . We compute the self-energy  $\Sigma^\Lambda$  in the presence of  $\phi_j$  within the same approximation as previously. It is thus determined from the flow equation (16) with a frequency-independent two-particle vertex  $\Gamma^\Lambda$ . Taking a derivative of that equation with respect to  $\phi_j$  at  $\phi_j = 0$  yields the flow equation for the response vertex

$$\frac{\partial}{\partial \Lambda} R_{j;1',1}^\Lambda = -\frac{1}{2\pi} \sum_{\omega=\pm\Lambda} \sum_{2,2'} \sum_{3,3'} \tilde{G}_{2,3'}^\Lambda(i\omega) R_{j;3',3}^\Lambda \tilde{G}_{3,2'}^\Lambda(i\omega) \Gamma_{1',2';1,2}^\Lambda . \quad (40)$$

Note that  $R_j^\Lambda$  is frequency-independent in our approximation and that there is no contribution from the  $\phi_j$ -derivative of  $\Gamma^\Lambda$ , since we neglect self-energy contributions in the flow of the two-particle vertex.

For spinless fermions with a (renormalized) nearest neighbor interaction, the matrix  $R_j^\Lambda$  is tridiagonal, that is only the components  $R_{j;l,l}^\Lambda$  and  $R_{j;l,l\pm 1}^\Lambda$  are non-zero, and their flow is given by

$$\begin{aligned} \frac{\partial}{\partial \Lambda} R_{j;l,l}^\Lambda &= -\frac{U^\Lambda}{2\pi} \sum_{\omega=\pm\Lambda} \sum_{l'} \sum_{r=\pm 1} \sum_{r'=0,\pm 1} \tilde{G}_{l+r,l'}^\Lambda(i\omega) R_{j;l',l'+r}^\Lambda \tilde{G}_{l'+r',l+r}^\Lambda(i\omega) \\ \frac{\partial}{\partial \Lambda} R_{j;l,l\pm 1}^\Lambda &= \frac{U^\Lambda}{2\pi} \sum_{\omega=\pm\Lambda} \sum_{l'} \sum_{r'=0,\pm 1} \tilde{G}_{l,l'}^\Lambda(i\omega) R_{j;l',l'+r'}^\Lambda \tilde{G}_{l'+r',l\pm 1}^\Lambda(i\omega) . \end{aligned} \quad (41)$$

The right hand sides involve only one unrestricted lattice summation, and can be computed in  $\mathcal{O}(L)$  time (see Appendix C). The initial condition for the response vertex is  $R_{j;l,\nu}^{\Lambda_0} = \delta_{jl}\delta_{l\nu}$ . The initial condition for the density is  $n_j^{\Lambda_0} = \frac{1}{2}$ , for any filling, due to the slow convergence of the flow equation (38) at large frequencies, which yields a finite contribution to the integrated flow from  $\Lambda = \infty$  to  $\Lambda_0$  for arbitrarily large finite  $\Lambda_0$ , as in the case of the self-energy discussed in more detail above.

To avoid the interference of Friedel oscillations emerging from the impurity or one boundary with those coming from the (other) boundaries of our systems we suppress the influence of the latter by coupling the finite chain to semi-infinite non-interacting leads, with a smooth decay of the interaction at the contacts. The presence of leads modifies the self-energy in the interacting region only via a boundary term. In particular, a lead coupled to the first site of the interacting region via nearest neighbor hopping (with amplitude  $t = 1$ ) yields the additional contribution

$$\Sigma_{j,j'}^{\text{lead}}(i\omega) = \frac{i\omega + \mu_0}{2} \left( 1 - \sqrt{1 - \frac{4}{(i\omega + \mu_0)^2}} \right) \delta_{1j}\delta_{jj'} \quad (42)$$

to the first diagonal element of self-energy matrix in real space.<sup>30</sup> Note that this term is frequency dependent and independent of  $\Lambda$ . A lead coupled to the last site yields an analogous contribution to the last diagonal element of the self-energy.

#### IV. RESULTS

We now present and discuss explicit results for the self-energy, spectral properties near the impurity or boundary, and the density profile, as obtained from the fRG. A comparison with exact DMRG results is made for the spectral weight at the Fermi level and for the density profile. Some fRG results for the self-energy and spectral properties of the spinless fermion model have been published already previously,<sup>14</sup> but only for half-filling and without any vertex renormalization. Here we present results also away from half-filling and demonstrate the quantitative improvement of accuracy obtained by including vertex renormalization. In addition we present for the first time fRG results for the density profile. Using a faster algorithm (see Appendix C) than previously we are now able to solve the flow equations for much larger systems.

The typical shape of the self-energy in the vicinity of an impurity can be seen in Fig. 5, where we plot the diagonal elements  $\Sigma_{j,j}$  and the off-diagonal elements  $\Sigma_{j,j+1}$  near a site impurity of strength  $V = 1.5$  added to the spinless fermion model with interaction strength  $U = 1$  at quarter-filling. Recall that the self-energy is tridiagonal in real space and frequency independent within our treatment. The diagonal elements can be interpreted as a local effective potential, the off-diagonal elements as a non-local effective potential which renormalizes the hopping amplitudes. At long distances from the impurity both  $\Sigma_{j,j}$  and

$\Sigma_{j,j+1}$  tend to a constant. The former describes just a bulk shift of the chemical potential, the latter a bulk renormalization of the hopping amplitude toward larger values. The oscillations around the bulk shifts are generated by the impurity. The wave number of the oscillations is  $2k_F = \pi/2$ , where  $k_F$  is the Fermi wave vector of the bulk system at quarter-filling. The amplitude of the oscillations of  $\Sigma$  decays slower than the inverse distance from the impurity at intermediate length scales, but approaches a decay proportional to  $1/|j-j_0|$  for  $|j-j_0| \rightarrow \infty$ . This can be seen most clearly by plotting an effective exponent  $\beta_j$  for the decay of the oscillations, defined as the negative logarithmic derivative of the oscillation amplitude with respect to the distance  $|j-j_0|$ . In Fig. 6 we show the effective exponent resulting from the oscillations of  $\Sigma_{j,j}$  as a function of the distance from a site impurity, for  $U = 1$  and half-filling. The impurity is situated at the center of a long chain with  $L = 2^{18} + 1$  sites. To avoid interferences with oscillations from the boundaries we have attached semi-infinite non-interacting leads to the ends of the interacting chain, as described in the last paragraph of III.C.2. Only for relatively large impurity strengths the asymptotic regime corresponding to  $\beta_j = 1$  is reached before finite size effects set in. For small  $V$  one can see that  $\beta_j$  increases from values below one, but the asymptotic long-distance behavior is cut off by the boundaries of the interacting region. For very small  $V$  (for example  $V = 0.01$  in Fig. 6) we observe a plateau in  $\beta_j$  for intermediate distances from the impurity site. In this regime  $\beta_j$  is close to  $K_\rho$  which can be understood by analytically solving our flow equations for small  $V$ .<sup>14</sup>

The long-range  $2k_F$ -oscillations of the self-energy lead to a marked suppression of the spectral weight for single-particle excitations at the Fermi level, that is at  $\omega = 0$ . In Fig. 7 we show the local density of states  $D_j(\omega)$  on the site next to a site impurity of strength  $V = 1.5$  for the spinless fermion model at half-filling. The result for the interacting system at  $U = 1$  is compared to the non-interacting case. Even-odd effects have been eliminated by averaging over neighboring eigenvalues (see Sec. III.C.1).  $\delta$ -peaks outside the band edges corresponding to bound states are not plotted. The interaction leads to a global broadening of the band, which is due to an enhancement of the bulk hopping amplitude, and also to a strong suppression of  $D_j(\omega)$  at low frequencies which is not present in the non-interacting system. For a finite system (here  $L = 1025$ ) the spectral weight at the Fermi level remains finite, but tends to zero with increasing system size. In Fig. 8 we show results for the density of states choosing the same parameters as in Fig. 7, but now for densities away from half-filling:  $n = 1/4$  and  $n = 3/4$ . In addition to the dip near  $\omega = 0$  a second singularity appears at a finite frequency. This effect is due to the fact that a long-range potential with a wave number  $2k_F$  does not only strongly scatter states with momenta near  $k_F$ , but also those with momenta close to  $\pi - k_F$ . Indeed the singularity is situated at  $\omega = \epsilon_{\pi-k_F} - \mu$ , where  $\epsilon_k$  is the renormalized (bulk) dispersion. In the half-filled case only one singularity is seen simply because  $\pi - k_F = k_F$  for  $k_F = \pi/2$ .

The spectral weight at the Fermi level is expected to vanish asymptotically as a power-law  $L^{-\alpha_B}$  with increasing system size, where  $\alpha_B = K_\rho^{-1} - 1$  is the *boundary exponent*

describing the power-law suppression of the density of states at the boundary of a semi-infinite chain.<sup>7</sup> That exponent depends only on the bulk parameters of the model, not on the impurity strength. For the spinless fermion model it can be computed exactly from the Bethe ansatz solution.<sup>25</sup> We therefore analyze the asymptotic behavior of the spectral weight at the Fermi level by defining an effective exponent  $\alpha(L)$  as the negative logarithmic derivative of the spectral weight with respect to the system size, such that  $\alpha(L)$  tends to a (positive) constant in case of a power-law suppression. In Fig. 9 we show results for  $\alpha(L)$  as obtained from the fRG for the spinless fermion model at quarter-filling with up to about  $10^6$  sites, for a weak ( $U = 0.5$ ) and an intermediate ( $U = 1.5$ ) interaction parameter. The spectral weight has been computed either at a boundary, or near a hopping impurity of strength  $t' = 0.5$ . Results obtained from the RG without (upper panel) and with (lower panel) vertex renormalization are compared to exact DMRG results (for up to 512 sites) and the exact boundary exponents  $\alpha_B$ , plotted as horizontal lines. The fRG results follow a power-law for large  $L$ , with the same asymptotic exponent for the boundary and impurity case, confirming thus the expected universality. However, the asymptotic regime is reached only for fairly large systems, even for the intermediate interaction strength  $U = 1.5$ . The comparison with the exact DMRG results and exact exponents shows that the fRG is also quantitatively rather accurate, and that the inclusion of vertex renormalization leads to a substantial improvement at intermediate coupling strength. Results for the effective exponent  $\alpha$  in the case of a site impurity are shown in Fig. 10, at quarter-filling and for an interaction strength  $U = 1$ . The comparison of the different curves obtained for different impurity strengths confirms once again the expected asymptotic universality, and also how the asymptotic regime shifts rapidly toward larger systems as the bare impurity strength decreases.

We finally discuss results for the density profile  $n_j$ . Boundaries and impurities induce Friedel oscillations of the local density with a wave vector  $2k_F$ . In a non-interacting system these oscillations decay proportionally to the inverse distance from the boundary or impurity. In an interacting Luttinger liquid the Friedel oscillations are expected to decay as  $|j - j_0|^{-K_\rho}$  at long distances  $|j - j_0|$ . For a very weak impurity one expects a slower decay proportional to  $|j - j_0|^{1-2K_\rho}$  at intermediate distances, and a crossover to the asymptotic power-law with exponent  $K_\rho$  at very long distances.<sup>28</sup> At intermediate distances the response of the density to a weak impurity can be treated in linear response theory, such that the density modulation is determined by the density-density response function at  $2k_F$ , which leads to the power-law decay with exponent  $2K_\rho - 1$ . In Fig. 11 we show fRG and DMRG results for the density profile  $n_j$  for a spinless fermion chain with 128 sites and interaction strength  $U = 1$  at half-filling. The Friedel oscillations emerge from both boundaries and interfere in the center of the chain. The accuracy of the RG results is excellent for all  $j$ . For incommensurate filling factors the density profile looks more complicated. This can be seen in Fig. 12, where functional RG results are shown for the density modulation  $|n_j - n|$  near the boundary of a system with an average density



$n = 0.393$  and 8192 sites. For long distances from the boundary the oscillation amplitude has a well-defined envelope which fits to a power-law as a function of  $j$ . We now analyze the long-distance behavior of the amplitudes more closely for the half-filled case, and compare to exact results for the asymptotic exponents. In Fig. 13 we show fRG results for the amplitude of density oscillations emerging from an open boundary, for a very long spinless fermion chain with  $2^{19} + 1$  sites and various interaction strengths  $U$  at half-filling. The other end of the chain (opposite to the open boundary) is smoothly connected to a non-interacting lead. In a log-log plot (upper panel of Fig. 13) the amplitude follows a straight line for almost all  $j$ , corresponding to a power-law dependence. Deviations from a perfect power-law can be seen more neatly by plotting the effective exponent  $\alpha_j$ , defined as the negative logarithmic derivative of the amplitude with respect to  $j$  (see the lower panel of Fig. 13). The effective exponent is almost constant except at very short distances or when  $j$  approaches the opposite end of the interacting chain, which is not surprising. From a comparison with the exact exponent (horizontal lines in the figure) one can assess the quantitative accuracy of the fRG results. Effective exponents describing the decay of Friedel oscillations generated by site impurities of various strengths are shown in Fig. 14, for a half-filled spinless fermion chain with  $2^{18} + 1$  sites and interaction  $U = 1$ . Both ends of the interacting chains are coupled to non-interacting leads to suppress oscillations coming from the boundaries. For strong impurities the results are close to the boundary result (cf. Fig. 13), as expected. For weaker impurities the oscillations decay more slowly, that is with a smaller exponent, and approach the boundary behavior only asymptotically at large distances (beyond the range of our chain for  $V < 1$ ). For very weak impurities ( $V = 0.01$  in Fig. 14) the oscillation amplitude follows a power-law corresponding to the linear response behavior with exponent  $2K_\rho - 1$  at intermediate distances. We finally present some results for the effective exponent of the density oscillation decay in the case of an *attractive* interaction  $U = -1$ , see Fig. 15. In that case the effective impurity strength should scale to zero at low energies and long distances.<sup>7</sup> Indeed, for weak and moderate bare impurity potentials the effective exponent in Fig. 15 approaches the linear density response exponent  $2K_\rho - 1$ . Only for very strong impurities the density oscillations decay with the smaller boundary exponent over several length scales.

## V. CONCLUSION

In summary, we have shown that the fRG provides an ideal tool for computing the intriguing properties of Luttinger liquids with static impurities. The method yields "ab initio" results for microscopic model systems at all energy scales from the Fermi energy to the ultimate low energy limit. We have demonstrated the power of the method by computing spectral properties of single-particle excitations as well as the oscillations in the density profile induced by impurities or boundaries for a spinless fermion model with nearest neighbor interaction. With the inclusion of vertex renormalization, in addition to

the renormalization of the effective impurity potential, our results agree remarkably well with exact asymptotic results and numerical DMRG data even for intermediate interaction strength.

There is a broad range of interesting further applications and extensions of the fRG for impurities in Luttinger liquids beyond the scope of the present article:

*Spin- $\frac{1}{2}$  fermions:* The inclusion of spin degrees of freedom requires a parametrization of the two-particle vertex with several coupling constants. We have already derived flow equations for the (extended) Hubbard model, with an effective vertex parametrized by local and nearest neighbor interactions.<sup>23</sup>

*Feedback of impurities on vertex:* For isolated impurities the influence of impurities on the vertex renormalization is irrelevant for the asymptotic low energy or long distance behavior, although it may contribute quantitatively at intermediate scales. In the case of disordered systems with a finite impurity density the influence of the latter on the two-particle vertex is crucial and must be taken into account.<sup>26</sup> In principle this is possible by computing the vertex flow with full propagators, which contain the renormalized impurity potential via the self-energy.

*Finite temperature:* The fRG approach can be extended without major complications to finite temperature. This is particularly useful for studying the temperature dependence of transport properties.<sup>30</sup>

*Transport:* In the absence of inelastic processes ( $\text{Im}\Sigma = 0$ ) the conductance of the interacting wire can be computed from the one-particle Green function in the presence of leads.<sup>30</sup> Several results have already been presented in short articles.<sup>19,20,21</sup>

*Inelastic processes:* Inelastic processes appear at second order in the interaction and can be included in the flow equations by inserting the second order vertex into the flow equation for the self-energy without neglecting its frequency dependence. This procedure would also capture the anomalous dimension of the bulk system, which is missing in the present work.

## Acknowledgements:

We are grateful to Manfred Salmhofer for useful discussions. This work benefitted from the workshop "Realistic theories of correlated electron materials" in fall 2002 at ITP-UCSB. V.M. thanks the Bundesministerium für Bildung und Forschung for financial support.

## APPENDIX A: EVALUATION OF VERTEX FLOW

Here we sketch some details concerning the explicit evaluation of the flow equations for the 2-particle vertex. Inserting the momentum structure of  $\Gamma^\Lambda$ , (24), into the flow

equation (26) and replacing  $g^\Lambda$  by  $U^\Lambda$  on the left hand side yields

$$\frac{\partial U^\Lambda}{\partial \Lambda} = \frac{(U^\Lambda)^2}{2\pi \sin^2 k_F} \sum_{\omega=\pm\Lambda} \int_0^{2\pi} \frac{dp}{2\pi} f(p, \omega) \quad (\text{A1})$$

where

$$f(p, \omega) = \frac{2 \sin^2 k_F \sin^2 p}{(i\omega - \xi_p^0)(-i\omega - \xi_{-p}^0)} - \frac{(\cos k_F - \cos p)^2}{(i\omega - \xi_p^0)^2} + \frac{[\cos(2k_F) - \cos p]^2}{(i\omega - \xi_{p-k_F}^0)(i\omega - \xi_{p+k_F}^0)}. \quad (\text{A2})$$

Here  $\xi_k^0 = -2 \cos k - \mu_0$  with  $\mu_0 = -2 \cos k_F$  is the bare dispersion relation relative to the bare Fermi level. Since  $f(p, \omega)$  can be written as a rational function of  $\cos p$  and  $\sin p$ , the  $p$ -integral can be carried out analytically using the substitution  $z = e^{ip}$  and the residue theorem. After a lengthy but straightforward calculation one obtains the following result for the coefficient  $h(\Lambda)$  in (28):

$$h(\Lambda) = -\frac{1}{2\pi} - \text{Re} \left[ \frac{i}{2} (\mu_0 + i\Lambda) \sqrt{1 - \frac{4}{(\mu_0 + i\Lambda)^2}} \right. \\ \left. \times \frac{3i\mu_0^4 - 10\mu_0^3\Lambda - 12i\mu_0^2(\Lambda^2 + 1) + 6\Lambda^3\mu_0 + 18\Lambda\mu_0 + 6i\Lambda^2 + i\Lambda^4}{\pi(2\mu_0 + i\Lambda)(4 - \mu_0^2 + \Lambda^2 - 2i\Lambda\mu_0)^2} \right]. \quad (\text{A3})$$

At half-filling ( $\mu_0 = 0$ ), this reduces to

$$h(\Lambda) = -\frac{1}{2\pi} \left[ 1 - \Lambda \frac{6 + \Lambda^2}{(4 + \Lambda^2)^{3/2}} \right]. \quad (\text{A4})$$

## APPENDIX B: CALCULATION OF $K_\rho$

In this appendix we show how the Luttinger liquid parameter  $K_\rho$ , which determines the critical exponents of Luttinger liquids, can be computed from the fixed point couplings as obtained from the RG. A comparison of the RG result for  $K_\rho$  with the exact Bethe ansatz result for the bulk model (without impurity) serves also as a check for the accuracy of our vertex renormalization. A relation between the fixed point couplings and  $K_\rho$  can be established via the exact solution of the fixed point Hamiltonian of Luttinger liquids, the Luttinger model.

For spinless fermions,  $K_\rho$  is determined by the Luttinger model parameters  $g$  and  $v_F$  as

$$K_\rho = \sqrt{\frac{1 - g/(2\pi v_F)}{1 + g/(2\pi v_F)}} \quad (\text{B1})$$

where  $g$  is the interaction between left and right movers and  $v_F$  the effective Fermi velocity of the model, that is the slope of the (linear) dispersion relation, with a possible shift due to interactions between particles moving in the same direction ( $g_4$ -coupling) already included.<sup>2</sup> We therefore need to extract  $g$  and  $v_F$  from the RG flow in the limit  $\Lambda \rightarrow 0$ .

In order to obtain  $K_\rho$  correctly to order  $U^2$ , it is sufficient to obtain  $v_F$  correctly to linear order in  $U$ .

The Luttinger model interaction  $g$  and the fixed point coupling  $g^* = \Gamma_{k_F, -k_F; k_F, -k_F}^{\Lambda \rightarrow 0}$  from the RG are not simply identical, in contrast to what one might naively expect. To find the true relation between  $g$  and  $g^*$ , one has to take into account that the forward scattering limit of the dynamical 2-particle vertex is generally not unique (in the absence of cutoffs), and depends on whether momentum or frequency transfers tend to zero first. This ambiguity is well-known in Fermi liquid theory, where it leads to the distinction between quasi-particle interactions and scattering amplitudes,<sup>27</sup> but is equally present in Luttinger liquids, for the same reason in all cases: the ambiguity of the small momentum, small frequency limit of particle-hole propagators contributing to the vertex function. In the *dynamical limit*, where the momentum transfer  $q$  vanishes first, the singular particle-hole propagators do not contribute. In Fermi liquids this limit yields the quasi-particle interaction. In the opposite *static limit* the frequency transfer  $\nu$  vanishes first and particle-hole propagators yield a finite contribution. In the presence of an infrared cutoff  $\Lambda > 0$  the forward scattering limit of the vertex function is unique, since the ambiguity in the particle-hole propagator is due to the infrared pole of the single-particle propagator. Hence  $\Gamma_{k_F, -k_F; k_F, -k_F}^\Lambda$  is well defined. However,  $\Gamma_{k_F, -k_F; k_F, -k_F}^\Lambda$  and also its limit for  $\Lambda \rightarrow 0$  depend on the choice for the cutoff function. For a momentum cutoff, which excludes states with excitation energies below  $\Lambda$  around the Fermi points, particle-hole excitations with small momentum transfers  $q$  are impossible. Hence particle-hole propagators with infinitesimal  $q$  do not contribute to the vertex at any  $\Lambda > 0$ , such that  $\Gamma_{k_F, -k_F; k_F, -k_F}^\Lambda$  converges to the dynamical forward scattering limit, which is simply given by the bare coupling constant  $g$  in the Luttinger model. For a frequency cutoff the particle-hole propagators with vanishing momentum and frequency transfer yield a finite contribution at  $\Lambda > 0$ , which tends to the static limit for  $\Lambda \rightarrow 0$ . This can be seen directly by integrating  $\sum_{\omega=\pm\Lambda} \int dp [G_p^0(i\omega)]^2$  over  $\Lambda$  from infinity to zero. Hence the vertex  $\Gamma_{k_F, -k_F; k_F, -k_F}^\Lambda$  obtained from our frequency cutoff RG tends to the *static* forward scattering limit.

For the Luttinger model, the static forward scattering limit of the vertex can be obtained from the dynamical effective interaction between left and right movers  $D(q, i\nu)$ , which is defined as the sum of particle-hole chains

$$D(q, i\nu) = g + g \Pi_-^0(q, i\nu) g \Pi_+^0(q, i\nu) g + \dots = \frac{g}{1 - g^2 \Pi_-^0(q, i\nu) \Pi_+^0(q, i\nu)} \quad (\text{B2})$$

where

$$\Pi_\pm^0(q, i\nu) = \pm \frac{1}{2\pi} \frac{q}{i\nu \mp v_F q} \quad (\text{B3})$$

is the bare particle-hole bubble for right (+) and left (-) movers. Note that only odd powers of  $g$  contribute to the effective interaction between left and right movers. This effective interaction appears naturally in the exact solution of the Luttinger model via

Ward identities.<sup>31</sup> For the static limit one obtains

$$\lim_{q \rightarrow 0} D(q, 0) = \frac{g}{1 - [g/(2\pi v_F)]^2} \quad (\text{B4})$$

which we identify with our fixed point coupling  $g^*$  as obtained from the RG with frequency cutoff. Inverting this relation between  $g$  and  $g^*$  we obtain

$$g = \frac{2\pi v_F}{g^*} \left[ -\pi v_F + \sqrt{(\pi v_F)^2 + (g^*)^2} \right] \quad (\text{B5})$$

For spinless fermions the difference between  $g$  and  $g^*$  appears only at third order in the coupling, but for models with spin the distinction becomes important already at second order.

The Fermi velocity  $v_F$  can be computed from the (frequency independent) self-energy in momentum space as

$$v_F = v_F^0 + \partial_k \Sigma_k|_{k_F}, \quad (\text{B6})$$

where  $v_F^0 = \partial_k \epsilon_k|_{k_F}$  is the bare Fermi velocity. The self-energy is computed from the flow equation (32), which can be rewritten in momentum space as

$$\frac{\partial}{\partial \Lambda} \Sigma_k^\Lambda = -\frac{U^\Lambda}{\pi} \sum_{\omega=\pm\Lambda} \int \frac{dp}{2\pi} \frac{1 - \cos(k-p)}{i\omega - \xi_p - \Sigma_p^\Lambda} \quad (\text{B7})$$

where  $\xi_p = \epsilon_p - \mu$ . The chemical potential  $\mu$  has to be fixed by the final condition  $\xi_{k_F} + \Sigma_{k_F} = 0$ , where  $k_F = \pi n$  depends only on the density, not the interaction. From the tridiagonal structure of  $\Sigma$  in real space, but also from the above expression it follows that  $\Sigma_k^\Lambda$  has the form  $\Sigma_k^\Lambda = a^\Lambda + b^\Lambda \cos k$ . The functional flow equation for  $\Sigma_k^\Lambda$  yields a coupled set of ordinary flow equations for the coefficients  $a^\Lambda$  and  $b^\Lambda$ , with initial conditions  $a^{\Lambda_0} = U$  and  $b^{\Lambda_0} = 0$ . The momentum integrals can be evaluated analytically via the residue theorem, such that the remaining set of two coupled differential equations (with  $U^\Lambda$  as input) can be easily solved numerically. The result for  $v_F$  is correct at least to first order in  $U$ , but not necessarily to second order, since our simplified parametrization captures the 2-particle vertex correctly to second order only at the Fermi points.

Inserting  $g$  and  $v_F$  into the Luttinger model formula (B1) we can now compute  $K_\rho$  as a function of  $U$  and density for the microscopic spinless fermion model. In Fig. 16 we show results for  $K_\rho(U)$  for various fixed densities, which are compared to the exact result from the Bethe ansatz solution<sup>25</sup> in the inset. The RG results are indeed correct to order  $U^2$  for small  $U$ , as expected, and they are surprisingly accurate also for larger values of  $U$ .

### APPENDIX C: NUMERICAL SOLUTION OF $\Sigma$ FLOW

For  $\Lambda < \Lambda_0 < \infty$  the flow equation for the self-energy (16) can be written as

$$\frac{\partial}{\partial \Lambda} \Sigma_{1',1}^\Lambda = -\frac{1}{2\pi} \sum_{2,2'} \Gamma_{1',2';1,2}^\Lambda \cdot 2 \text{Re} \left[ \tilde{G}_{2,2'}^\Lambda(i\Lambda) \right]. \quad (\text{C1})$$

In order to compute its right-hand side, one needs to invert the tridiagonal matrix

$$T = G_0^{-1}(i\Lambda) - \Sigma^\Lambda, \quad (\text{C2})$$

where  $T$  is complex symmetric (*not* hermitean) with diagonal elements  $a_i := i\Lambda + \mu - \Sigma_{i,i}^\Lambda$ ,  $i = 1, \dots, L$ , and first off-diagonal elements  $b_i := t - \Sigma_{i,i+1}^\Lambda$ ,  $i = 1, \dots, L-1$ . Note that  $\text{Im}(a_i) = \Lambda > 0$  such that  $T$  is non-singular and its inverse well-defined.

The inverse  $\tilde{G}^\Lambda(i\Lambda) = T^{-1}$  is not tridiagonal but a full matrix which can be computed by standard methods in  $\mathcal{O}(L^2)$  time. However, for an interaction that does not extend beyond nearest neighbors on the lattice, only the tridiagonal part of  $\tilde{G}$  is required, which can be computed in  $\mathcal{O}(L)$  time, such that much larger lattices can be treated. We shall first explain how this is done and then present the resulting algorithm that can directly be incorporated into a computer program.

Under certain assumptions (see below), a matrix can be uniquely factorized into a lower unit triangular matrix  $L$ , a diagonal matrix  $D$ , and an upper unit triangular matrix  $U$  (“LDU factorisation”):  $T = L \cdot D \cdot U$ .<sup>32</sup> For a tridiagonal matrix  $T$  the unit triangular matrices  $L$  and  $U$  are in fact unit bidiagonal: their matrix elements are one on the diagonal, and only the first off-diagonal is nonzero. Since our  $T$  is symmetric we have  $L = U^T$ . Thus we obtain a factorization of the form

$$T = U^{+T} D^+ U^+ = \begin{pmatrix} 1 & & & \\ U_1^+ & 1 & & \\ & U_2^+ & 1 & \\ & & \ddots & \ddots \end{pmatrix} \begin{pmatrix} D_1^+ & & & \\ & D_2^+ & & \\ & & D_3^+ & \\ & & & \ddots \end{pmatrix} \begin{pmatrix} 1 & U_1^+ & & \\ & 1 & U_2^+ & \\ & & 1 & \ddots \\ & & & \ddots \end{pmatrix}$$

where the label “+” distinguishes this factorization from another one used below. The prescription to compute the elements  $D_i^+$  and  $U_i^+$  is well known and can be found for example in Ref.<sup>32</sup>. Starting in the upper left corner one proceeds to increasing row and column numbers until one arrives at the lower right corner of  $T$ :

$$D_1^+ := a_1, \quad U_i^+ := b_i/D_i^+, \quad D_{i+1}^+ := a_{i+1} - b_i U_i^+ \quad (i = 1, \dots, L-1). \quad (\text{C3})$$

This works well since in our case  $\text{Im}(D_i^+) \geq \Lambda > 0$ , such that one never divides by zero.

To compute the inverse  $\tilde{G} = T^{-1}$ , one could directly calculate  $(U^+)^{-1}(D^+)^{-1}(U^{+T})^{-1}$ . It is however easier and more accurate to find the inverse by solving the linear system of equations  $T\tilde{G} = 1$ , where 1 is the identity matrix, by “backsubstitution”. To be specific, consider the  $i^{\text{th}}$  column vector  $\tilde{G}_{\cdot,i}$  of  $\tilde{G}$ :

$$e_i = T\tilde{G}_{\cdot,i} = U^{+T}(D^+U^+\tilde{G}_{\cdot,i}) = U^{+T}g_i, \quad U^+\tilde{G}_{\cdot,i} = (D^+)^{-1}g_i \quad (\text{C4})$$

where  $e_i$  is the  $i^{\text{th}}$  unit vector. The first step is to solve the linear system  $U^{+T}g_i = e_i$  for  $g_i$ , and the second step to solve  $U^+\tilde{G}_{\cdot,i} = (D^+)^{-1}g_i$  for  $\tilde{G}_{\cdot,i}$ . To solve a tridiagonal

linear system for one vector takes  $\mathcal{O}(L)$  time, so solving for the full inverse matrix  $\tilde{G}$  takes  $\mathcal{O}(L^2)$  time.

Now we shall derive an algorithm to compute the elements of  $g_i$  and  $\tilde{G}_{\cdot,i}$ . Begin with the last column  $i = L$ :  $U^{+T}g_L = e_L$  can be solved from the first to the last row and gives  $g_L = e_L$ . Next  $U^+\tilde{G}_{\cdot,L} = (D^+)^{-1}e_L$  can be solved starting from the last row,  $\tilde{G}_{L,L} = 1/D_L^+$ . From there one can work upwards by backsubstitution,  $\tilde{G}_{j,L} = -U_j^+\tilde{G}_{j+1,L}$  ( $j = 1, \dots, L-1$ ). For the other columns  $i < L$ , one cannot take the shortcut and has to solve both linear systems for  $g_i$  and  $\tilde{G}_{\cdot,i}$ . But it is now important to realize that for any column vector  $\tilde{G}_{\cdot,i+1}$ , if we somehow know the diagonal element  $\tilde{G}_{i+1,i+1}$ , the next element above the diagonal is

$$\tilde{G}_{i,i+1} = -U_i^+\tilde{G}_{i+1,i+1} \quad (i = 1, \dots, L-1). \quad (\text{C5})$$

Thus we have a prescription how to go up one row in  $\tilde{G}$ . Together with the symmetry of  $\tilde{G}$ , that is  $\tilde{G}_{i,i+1} = \tilde{G}_{i+1,i}$ , which follows from the symmetry of  $T$ , we get the first off-diagonal element one column to the left *without* solving the two linear systems in (C4). So it is possible to compute directly the tridiagonal part of the inverse. However, there is another algorithm which is much more accurate for near-singular matrices at the end of the RG flow: the double factorization.<sup>33</sup> It does not rely on the symmetry of  $\tilde{G}$  but uses the complementary “UDL” factorization

$$T = U^- D^- L^- = U^- D^- U^{-T}, \quad (\text{C6})$$

where the matrix elements are obtained as

$$D_L^- := a_L, \quad U_i^- := b_i/D_{i+1}^-, \quad D_i^- := a_i - b_i U_i^- \quad (i = L-1, \dots, 1). \quad (\text{C7})$$

We proceed as for the LDU factorization above and get

$$\tilde{G}_{1,1} = 1/D_1^- \quad (\text{C8})$$

$$\tilde{G}_{i,i+1} = -U_i^- \cdot \tilde{G}_{i,i}. \quad (\text{C9})$$

We can combine equations (C5) and (C9) to relate consecutive diagonal elements:

$$\tilde{G}_{i+1,i+1} = -\tilde{G}_{i,i+1}/U_i^+ = \tilde{G}_{i,i} \cdot U_i^-/U_i^+ = \tilde{G}_{i,i} \cdot D_i^+/D_{i+1}^- . \quad (\text{C10})$$

Thus we start with (C8) and use the  $U^- D^- L^-$  decomposition to go one matrix element to the right in the inverse matrix, from the diagonal to the first off-diagonal (C9), while the  $L^+ D^+ U^+$  decomposition allows to go down by one, back to the next diagonal element (C5). There is no need to compute the full inverse matrix.

One can implement the algorithm without knowing the derivation by using equations (C3) and (C7) - (C10). One can further eliminate the  $U$ 's using equations (C3) and (C7) and implement the algorithm such that only the input vectors  $a_i$ ,  $b_i$  and the output

vectors  $\tilde{G}_{i,i}$ ,  $\tilde{G}_{i,i+1}$  enter the temporary storage. This double factorization is numerically accurate to more than 10 significant digits (using double precision) even for large lattices ( $10^6$  sites) and almost singular matrices with  $|a_i| \sim 10^{-15}$  which appear at the end of the flow for half filling.

The right hand side of the flow equations (41) for the density response vertex  $R^\Lambda$  can be computed in  $\mathcal{O}(L)$  time using the fact that the upper triangular part of the inverse of a tridiagonal matrix (here  $\tilde{G}$ ) is the upper triangular part of the outer product of two vectors.<sup>33,34</sup>

- 
- <sup>1</sup> T. Giamarchi, *Quantum Physics in One Dimension* (Oxford University Press, New York, 2003).
  - <sup>2</sup> For a review on Luttinger liquids, see J. Voit, Rep. Prog. Phys. **58**, 977 (1995).
  - <sup>3</sup> A. Luther and I. Peschel, Phys. Rev. B **9**, 2911 (1974).
  - <sup>4</sup> D. C. Mattis, J. Math. Phys. **15**, 609 (1974).
  - <sup>5</sup> W. Apel and T.M. Rice, Phys. Rev. B **26**, 7063 (1982).
  - <sup>6</sup> T. Giamarchi and H.J. Schulz, Phys. Rev. B **37**, 325 (1988).
  - <sup>7</sup> C.L. Kane and M.P.A. Fisher, Phys. Rev. B **46**, 15233 (1992).
  - <sup>8</sup> S. Eggert and I. Affleck, Phys. Rev. B **46**, 10866 (1992).
  - <sup>9</sup> D. Yue, L.I. Glazman, and K.A. Matveev, Phys. Rev. B **49**, 1966 (1994).
  - <sup>10</sup> For a review on isolated impurities in Luttinger liquids, see Ref. [1], chapter 10.
  - <sup>11</sup> For a recent comprehensive review of the DMRG, see U. Schollwöck, to appear in Rev. Mod. Phys.
  - <sup>12</sup> M. Salmhofer, *Renormalization* (Springer, Berlin, 1998).
  - <sup>13</sup> First computational applications of the fRG to Fermi systems were performed for the 2D Hubbard model, see D. Zanchi and H.J. Schulz, Phys. Rev. B **61**, 13609 (2000); C.J. Halboth and W. Metzner, *ibid* **61**, 7364 (2000); C. Honerkamp, M. Salmhofer, N. Furukawa, and T. M. Rice, *ibid.* **63**, 035109 (2001).
  - <sup>14</sup> V. Meden, W. Metzner, U. Schollwöck, and K. Schönhammer, Phys. Rev. B **65**, 045318 (2002); J. Low Temp. Phys. **126**, 1147 (2002).
  - <sup>15</sup> C. Wetterich, Phys. Lett. B **301**, 90 (1993).
  - <sup>16</sup> T.R. Morris, Int. J. Mod. Phys. A **9**, 2411 (1994).
  - <sup>17</sup> For generic interacting Fermi systems, a concise derivation of the full hierarchy of flow equations is presented by M. Salmhofer and C. Honerkamp, Prog. Theor. Phys. **105**, 1 (2001).
  - <sup>18</sup> V. Meden and U. Schollwöck, Phys. Rev. B **67**, 035106 (2003).
  - <sup>19</sup> V. Meden and U. Schollwöck, Phys. Rev. B **67**, 193303 (2003).
  - <sup>20</sup> V. Meden, S. Andergassen, W. Metzner, U. Schollwöck, and K. Schönhammer, Europhys. Lett. **64**, 769 (2003).



- <sup>21</sup> V. Meden, T. Enss, S. Andergassen, W. Metzner, and K. Schönhammer, cond-mat/0403655 (unpublished).
- <sup>22</sup> Vertex renormalization has already been applied in two letters on transport properties, Ref. [20,21], but without any derivation of the method.
- <sup>23</sup> S. Andergassen, T. Enss, V. Meden, W. Metzner, U. Schollwöck, and K. Schönhammer (unpublished).
- <sup>24</sup> C.N. Yang and C.P. Yang, Phys. Rev. **150**, 321 (1966); *ibid* 327 (1966).
- <sup>25</sup> F.D.M. Haldane, Phys. Rev. Lett. **45**, 1358 (1980).
- <sup>26</sup> See, for example, T. Giamarchi and H. Maurey, in *Correlated Fermions and Transport in Mesoscopic Systems*, edited by T. Martin, G. Montambaux, and J. Tran Thanh Van (Editions Frontieres, Paris, 1997).
- <sup>27</sup> J.W. Negele and Orland, *Quantum Many-Particle Systems* (Addison-Wesley, Reading, 1987).
- <sup>28</sup> R. Egger and H. Grabert, Phys. Rev. Lett. **75**, 3505 (1995).
- <sup>29</sup> See, for example, J. Zinn-Justin, *Quantum Field Theory and Critical Phenomena* (Oxford University Press, New York, 1996).
- <sup>30</sup> The derivation will be given in an upcoming paper containing a detailed discussion of transport properties, see T. Enss, S. Andergassen, V. Meden, W. Metzner, U. Schollwöck, and K. Schönhammer (unpublished).
- <sup>31</sup> I.E. Dzyaloshinskii and A.I. Larkin, Zh. Eksp. Teor. Fiz. **65**, 411 (1973) [Sov. Phys. JETP **38**, 202 (1974)]; W. Metzner and C. Di Castro, Phys. Rev. B **47**, 16107 (1993).
- <sup>32</sup> See, for example, W.H. Press, S.A. Teukolsky, W.T. Vetterling, and B.P. Flannery, *Numerical Recipes in Fortran 77* (Cambridge Univ. Press, 1986).
- <sup>33</sup> For a pedagogical review on the inverse of symmetric tridiagonal matrices, see G. Meurant, SIAM J. Matrix Anal. Appl. **13**, 707 (1992).
- <sup>34</sup> For more details, see T. Enss, Ph.D. thesis, University of Stuttgart, 2004 (unpublished).

$$\frac{\partial}{\partial \Lambda} \Sigma^\Lambda = \text{Diagram: A shaded square vertex labeled } \Gamma^\Lambda \text{ with a circle (self-energy) attached to its top side, labeled } S^\Lambda.$$

FIG. 1: Flow equation for the selfenergy  $\Sigma^\Lambda$ .

$$\begin{aligned} \frac{\partial}{\partial \Lambda} \Gamma^\Lambda = & \text{Diagram: Two shaded square vertices labeled } \Gamma^\Lambda \text{ connected by two arcs, top labeled } S^\Lambda \text{ and bottom labeled } G^\Lambda. \\ & + \text{Diagram: A shaded hexagon vertex labeled } \Gamma_3^\Lambda \text{ with a circle (self-energy) attached to its top side, labeled } S^\Lambda. \end{aligned}$$

FIG. 2: Flow equation for the 2-particle vertex  $\Gamma^\Lambda$ .

$$\begin{aligned}
\frac{\partial}{\partial \Lambda} \Gamma^\Lambda = & \text{Diagram 1} \\
& - \text{Diagram 2} - \text{Diagram 3} \\
& + \text{Diagram 4} + \text{Diagram 5}
\end{aligned}$$

The diagrams represent Feynman diagrams for the flow equation of the 2-particle vertex. Diagram 1 is a box with two external legs (1, 2) and two internal legs (1', 2'). Diagrams 2 and 3 are similar but with different internal line connections. Diagrams 4 and 5 are similar but with different external line connections. The diagrams are arranged in a grid with minus and plus signs between them.

FIG. 3: Flow equation for the 2-particle vertex at 1-loop level with particle-particle and particle-hole channels written explicitly.

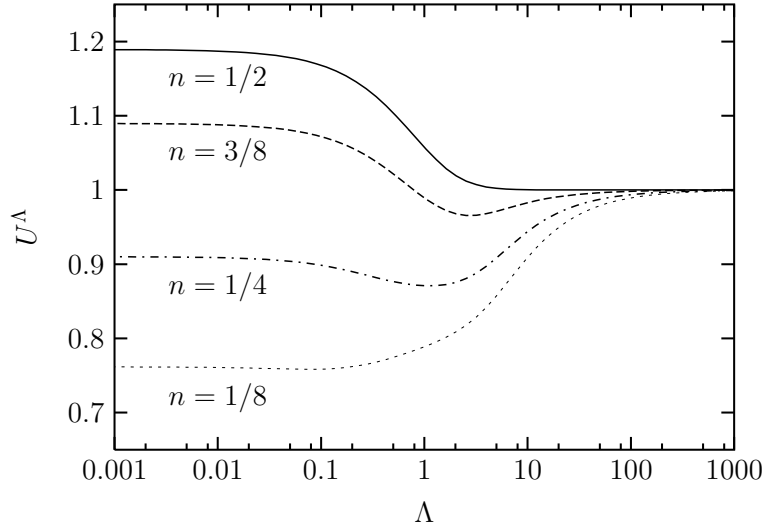


FIG. 4: Flow of the renormalized nearest neighbor interaction  $U^\Lambda$  for the spinless fermion model, for  $U = 1$  and various densities  $n$ .

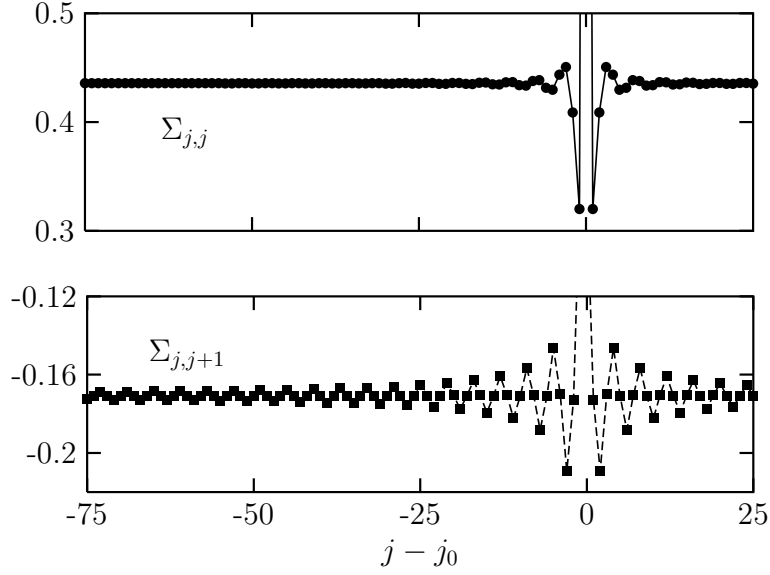


FIG. 5: Self-energy near a site impurity of strength  $V = 1.5$  for the spinless fermion model at quarter-filling and interaction strength  $U = 1$ ; the impurity is situated at the center of a chain with  $L = 1025$  sites.

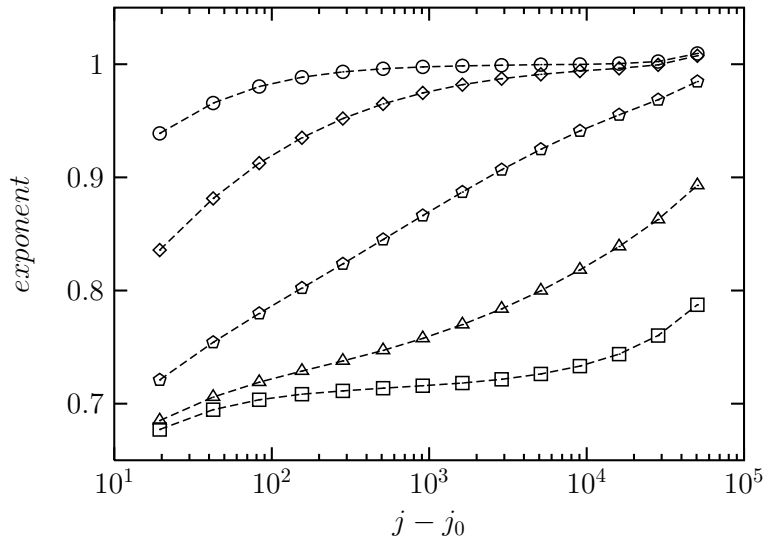


FIG. 6: Effective exponent for the decay of oscillations of  $\Sigma_{j,j}$  as a function of the distance from a site impurity of strengths  $V = 0.01, 0.1, 0.3, 1, 10$  (from bottom to top), for the spinless fermion model at half-filling and interaction strength  $U = 1$ ; the impurity is situated at the center of a chain with  $L = 2^{18} + 1$  sites.

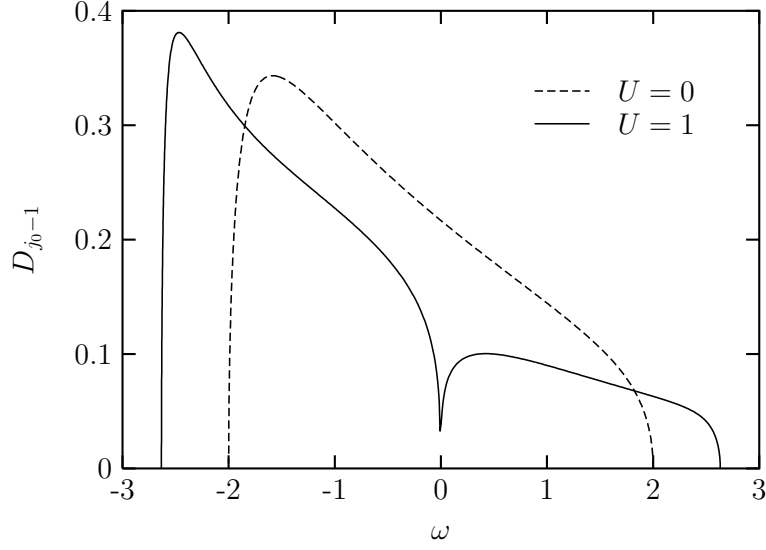


FIG. 7: Local density of states on the site next to a site impurity of strength  $V = 1.5$  for spinless fermions at half-filling and  $U = 1$ ; the impurity is situated at the center of a chain with  $L = 1025$  sites; the non-interacting case  $U = 0$  is shown for comparison.

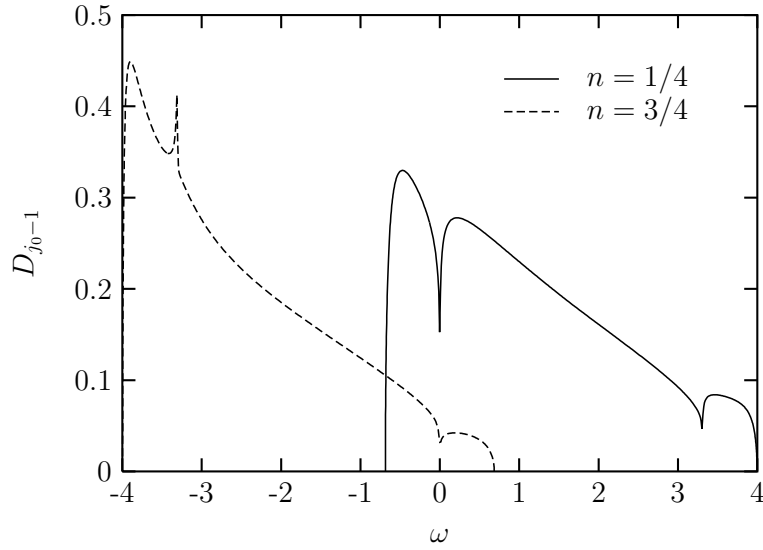


FIG. 8: Local density of states on the site next to a site impurity as in Fig. 7 (same parameters), but now for densities  $n = 1/4$  and  $n = 3/4$ .

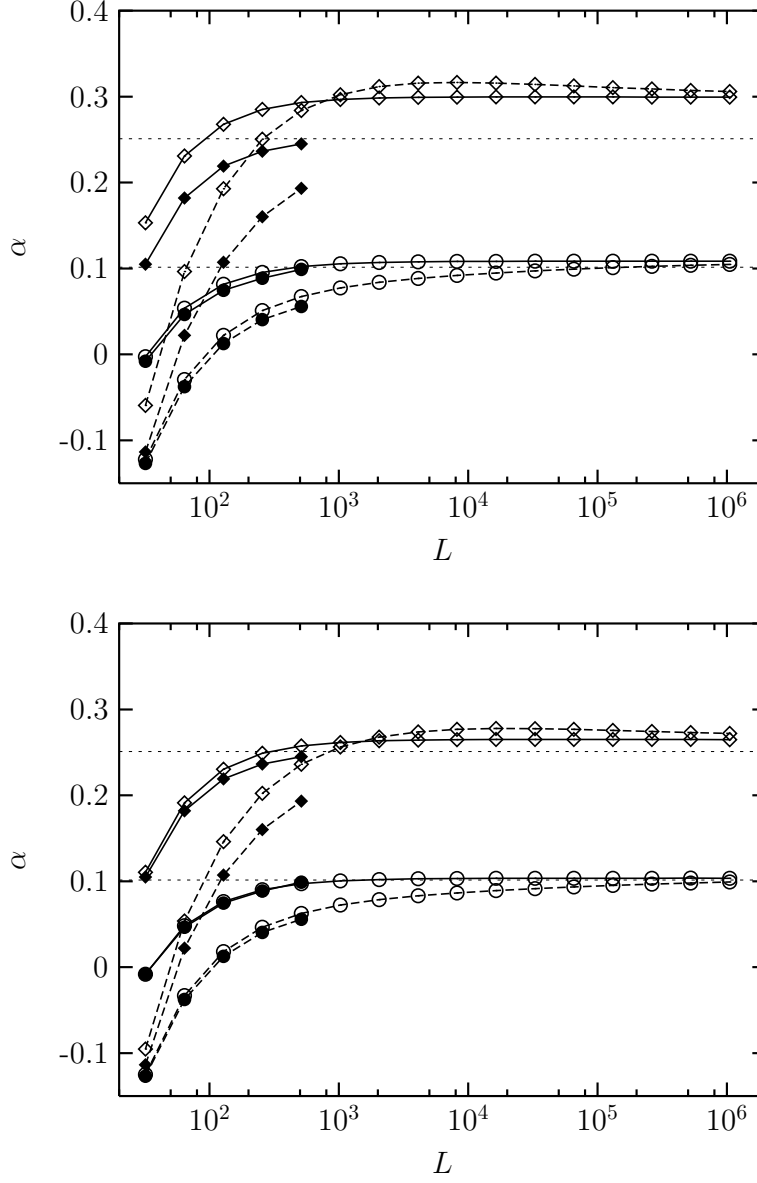


FIG. 9: Logarithmic derivative of the spectral weight at the Fermi level near a boundary (solid lines) or hopping impurity (dashed lines) as a function of system size  $L$ , for spinless fermions at quarter-filling and interaction strength  $U = 0.5$  (circles) or  $U = 1.5$  (squares); *upper panel*: without vertex renormalization, *lower panel*: with vertex renormalization; the open symbols are fRG, the filled symbols DMRG results; the horizontal lines represent the exact boundary exponents for  $U = 0.5$  and  $U = 1.5$ . In the boundary case (solid lines) the spectral weight has been taken on the first site of a homogeneous chain, in the impurity case (dashed lines) on one of the two sites next to a hopping impurity  $t' = 0.5$  in the center of the chain.

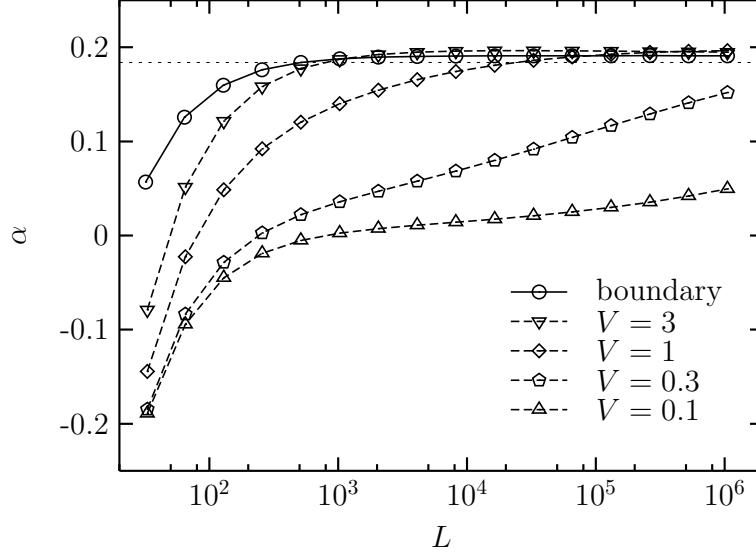


FIG. 10: Logarithmic derivative of the spectral weight at the Fermi level near a boundary (solid line) or near a site impurity (dashed lines) as a function of system size  $L$ , for spinless fermions at quarter-filling and interaction strength  $U = 1$ . In the boundary case the spectral weight has been taken on the first site of a homogeneous chain, in the impurity case on the site next to a site impurity of strength  $V$  in the center of the chain. The horizontal line represents the exact boundary exponent for  $U = 1$ .

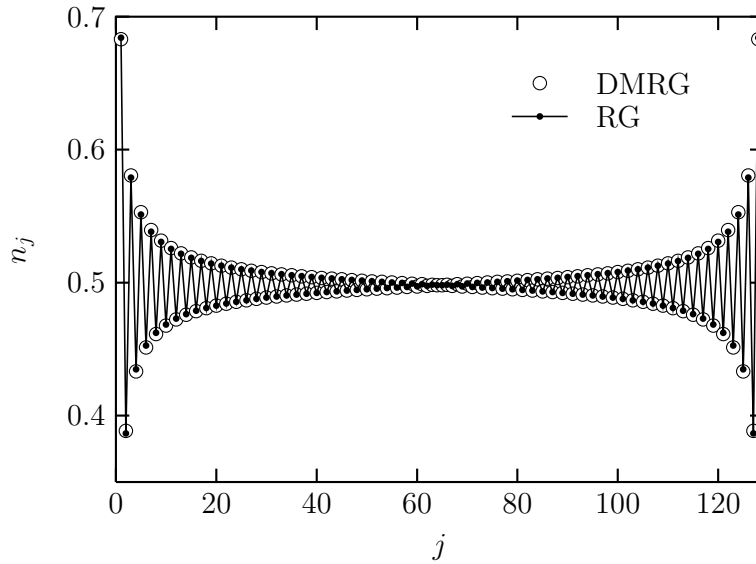


FIG. 11: Density profile  $n_j$  for a spinless fermion chain with 128 sites and interaction strength  $U = 1$  at half-filling; fRG results are compared to exact DMRG results.

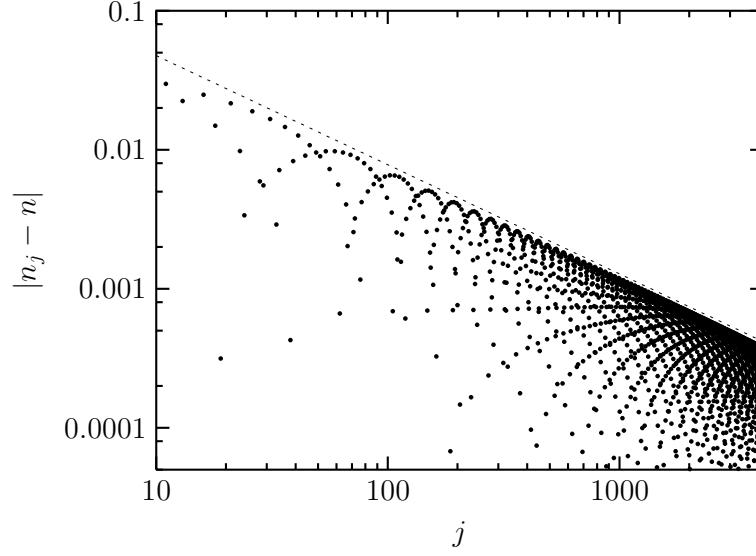


FIG. 12: Density modulation  $|n_j - n|$  as a function of the distance from a boundary, for spinless fermions with interaction strength  $U = 1$  and (average) density  $n = 0.393$  on a chain with 8192 sites; the broken straight line is a power-law fit to the envelope of the oscillation amplitudes.



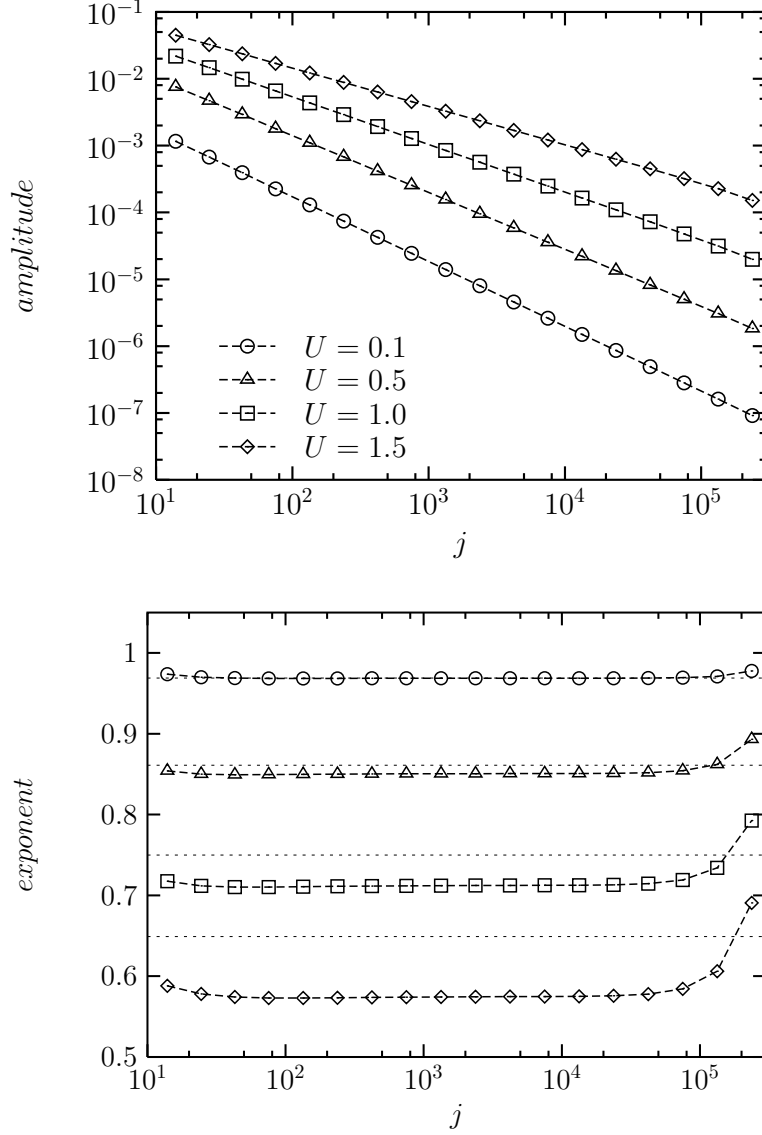


FIG. 13: Amplitude (envelope) of oscillations of the density profile  $n_j$  induced by a boundary as a function of the distance from the boundary, for spinless fermions with various interaction strengths  $U$  at half-filling; the interacting chain with  $2^{19} + 1$  sites is coupled to a semi-infinite non-interacting lead at one end (opposite to the boundary); *upper panel*: log-log plot of the amplitude, *lower panel*: effective exponents for the decay, and the exact asymptotic exponents as horizontal lines.

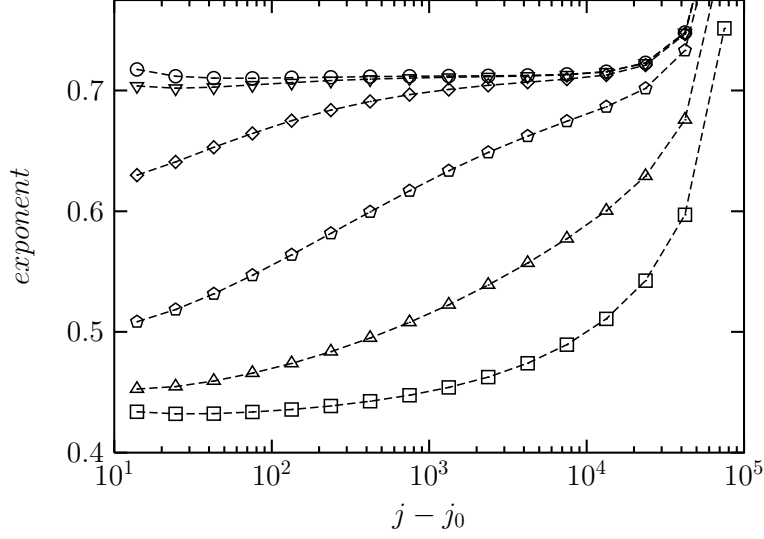


FIG. 14: Effective exponent for the decay of density oscillations as a function of the distance from a site impurity of strengths  $V = 0.01, 0.1, 0.3, 1, 3, 10$  (from bottom to top); the impurity is situated at the center of a spinless fermion chain with  $2^{18} + 1$  sites and interaction strength  $U = 1$  at half-filling; the interacting chain is coupled to semi-infinite non-interacting leads at both ends.

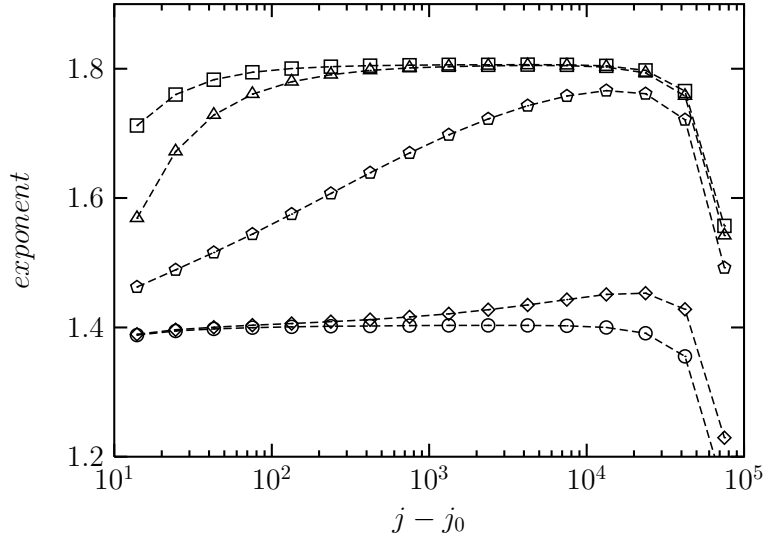


FIG. 15: Effective exponent for the decay of density oscillations as a function of the distance from a site impurity of strengths  $V = 0.1, 1, 10, 100, 1000$  (from top to bottom) for the same chain as in Fig. 14 but now with an *attractive* interaction,  $U = -1$ .

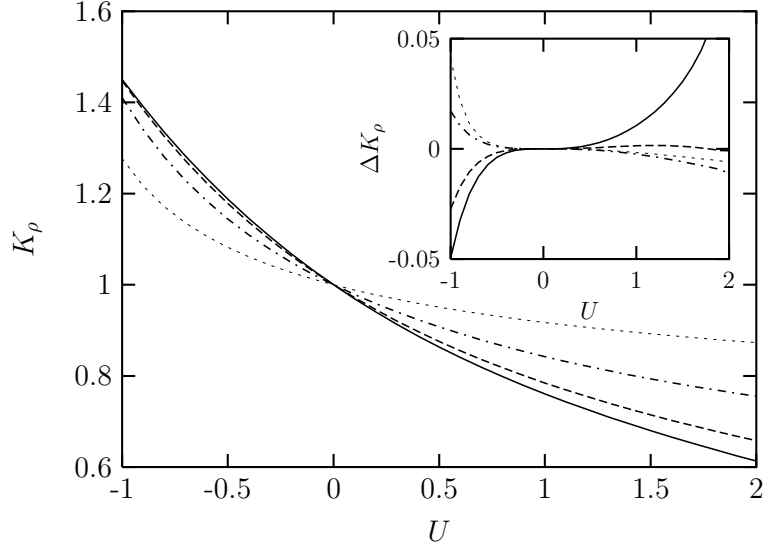


FIG. 16: Luttinger liquid parameter  $K_\rho$  as a function of  $U$  at various densities (as in Fig. 4) for the spinless fermion model; the inset shows the difference between the RG result and the exact Bethe ansatz result for  $K_\rho$ .